We are IntechOpen, the world's leading publisher of Open Access books Built by scientists, for scientists

4,800
Open access books available

122,000
International authors and editors

135M
Downloads

Our authors are among the

154
Countries delivered to

TOP 1%
most cited scientists

12.2%
Contributors from top 500 universities

CLARIVATE ANALYTICS BOOK CITATION INDEX INDEXED

WEB OF SCIENCE™

Selection of our books indexed in the Book Citation Index in Web of Science™ Core Collection (BKCI)

Interested in publishing with us?
Contact book.department@intechopen.com

Numbers displayed above are based on latest data collected.
For more information visit www.intechopen.com

12

Molecular Imaging of Tumor Angiogenesis

Shaunagh McDermott and Alexander Guimaraes
Massachusetts General Hospital,
USA

1. Introduction

Molecular imaging has recently been defined by the Society of Nuclear Medicine as 'the visualization, characterization, and measurement of biological processes at the molecular and cellular levels in humans and other living systems' (Mankoff 2007). It usually exploits specific labeled molecular probes, as well as intrinsic tissue characteristics as the source of image contrast, and uses a number of molecular imaging modalities, including magnetic resonance imaging, optical imaging, targeted ultrasound, single photon emission tomography and positron emission tomography (Massoud and Gambhir 2003).

Angiogenesis is the development of new vasculature from pre-existing blood vessels and/or circulating endothelial calls (Bergers and Benjamin 2003). It is well established that angiogenesis is one of the key aspects in the growth and metastasis of solid tumors (Folkman 1995; Ferrara and Kerbel 2005). Typically tumor-associated angiogenesis goes through two phases, an avascular and a vascular phase that are separated by the 'angiogenic switch'. The avascular phase of tumors corresponds to small and occult lesions that stay dormant and subsist on diffusion of nutrients from the host microvasculature. After reaching a certain size (usually around 1-2mm), a small subset of dormant tumors enter the vascular phase in which exponential tumor growth ensues. Angiogenesis is a complex multistep process regulated by many factors. At the onset of angiogenesis, a number of pro-angiogenic growth factors (e.g. vascular endothelial growth factors, platelet derived growth factor, fibroblast growth factors) and proteolytic enzymes (e.g. metalloproteinases, cathepsin cysteine proteases, plasmin) are secreted into the interstitium. This leads to degradation of basal membrane surrounding the pre-existing vasculature, along with proliferation and migration of smooth muscle and endothelial cells. All these events lead to the alignment and organization of endothelial cells to form new vessels and a vascular network within the tumor (Ferrara and Kerbel 2005).

Tumor angiogenesis is not simply the production of an increased number of blood vessels to serve a growing mass. Although the main purpose of tumor angiogenesis can be considered to maintain a cancer's blood supply, the process occurs in an unmitigated fashion, and the resultant vascular network is highly abnormal. This profoundly aberrant vasculature dramatically alters the tumor microenvironment and influences heavily the ways in which cancers grow and progress, escape the host's immune system, metastasize, and respond to anticancer therapies.

The heterogeneity in vessel distribution and haphazard anatomical arrangement of the vasculature cause spatial and temporal heterogeneity in blood flow, with areas of hypervasularity adjacent to hypovascular ones (Tong, Boucher et al. 2004). Also, the structural abnormalities of the tumor vasculature lead to a marked increase in vessel leakiness. As a consequence, there is a protein and fluid build-up in the tumor interstitium. This excess extravasation of protein increases the extravascular oncotic pressure, dragging further fluid into the interstitial space (Stohrer, Boucher et al. 2000; Tong, Boucher et al. 2004). Furthermore, there is an absence of functional intratumoral lymphatic vessels, resulting in the impaired clearance of extracellular fluid and hence interstitial hypertension within tumors. The raised intratumoral interstitial fluid pressure (IFP) reduces the hydrostatic pressure gradient between the intravascular and extravascular compartments such that the two essentially equilibrate, which reduces transvascular flow. Also, the mechanical stress from the solid mass of proliferating cancer cells and the matrix is able to collapse tumor vessels, closing the lumen through compressive forces (Padera, Stoll et al. 2004). This combination of regional poor perfusion, raised IFP, and areas of vascular collapse produces regional hypoxia and acidosis within tumors (Helmlinger, Yuan et al. 1997). Aberrations in the tumor vasculature have great implications for tumor sensitivity to therapy. Hypoxia is a well-known mediator of cancer cell resistance to conventional radiotherapy and cytotoxics (Teicher 1996; Wouters and Brown 1997). Moreover, the poor blood supply and raised intratumoral IFP (leading to a reduction in transvacular flow) impair the delivery of systemically administered therapies to tumors such as conventional cytotoxics and monoclonal antibodies (Jain 1989; Tong, Boucher et al. 2004).

With the discovery of vascular endothelial growth factor (VEGF) as a major driver of tumor angiogenesis, efforts were focused on novel therapeutics aimed at inhibiting VEGF activity, with the goal of regressing tumors by starvation. Unfortunately, clinical trials of anti-VEGF monotherapy in patients with solid tumors have been largely negative (Jain, Duda et al. 2006). Intriguingly, the combination of anti-VEGF therapy with conventional chemotherapy has improved survival in cancer patients compared with chemotherapy alone (Sandler, Gray et al. 2006; Saltz, Clarke et al. 2008). In 2001, a 'vascular normalization' hypothesis was proposed to explain this paradox (Jain 2001). The normalization hypothesis suggests that by correcting the abnormalities in structure and function of tumor vessels (rather than destroying vessels completely) we can normalize the tumor microenvironment and ultimately control tumor progression and improve response to other therapies (Jain 2005).

Non-invasive imaging of tumor angiogenesis will allow for much earlier detection of tumors and also the development of surrogate markers for assessing response to treatment.

2. Imaging of angiogenesis

Imaging angiogenesis has been focused into three different arenas: 1) kinetic imaging using dynamic tracking of contrast administration; 2) steady state blood volume determinations of neovascular density; and 3) specific molecular markers of angiogenesis.

2.1 Kinetic imaging using dynamic tracking of contrast material

Dynamic contrast-enhanced imaging is a noninvasive technique that can provide parameters related to tissue perfusion and permeability for examination of the tumor vasculature.

2.1.1 Dynamic contrast-enhanced ultrasound

Contrast-enhanced ultrasound (CEU) imaging is based on the reception, analysis and display of acoustic signals produced by reflection or backscatter of sound (echo) with use of contrast agents. The most commonly used contrast agent are microbubbles that are gas-liquid emulsions consisting of a gaseous core (e.g. perfluorocarbon, sulfur hexfluoride, or nitrogen) that is enclosed by a shell composed of biocompatible materials (albumin, galactose, lipids, polymers). The gaseous core of the microbubbles causes a very high echogenic response following insonification with ultrasound, resulting in high contrast-to-tissue background ratio. Owing to their micron size (usually ranging in size between 1 and 4 μm in diameter), these microbubbles stay within the vascular compartment, and do not leak out into the extra-vascular space (Deshpande, Pysz et al. 2010). Thus, microbubbles are highly suitable for imaging angiogenic markers that are over expressed on tumor vascular endothelial cells (Deshpande, Needles et al. 2010).

Following intravenous administration, microbubbles do not coalesce to form emboli, but dissolve leaving remnants that are easily metabolized or excreted. Further, biodistribution studies revealed that microbubbles have low circulation residence times as they are rapidly removed by the reticuloendothelial system (Perkins, Frier et al. 1997; Weskott 2008; Willmann, Cheng et al. 2008). To increase the circulation time of the microbubbles in serum, additional coatings, such as polyethylene glycol polymer arms are added onto the microbubble shell. Additionally these coatings help stabilize the microbubble by providing additional steric protection, preventing aggregation and help escape immune surveillance by the body (Klibanov 2009).

To make ultrasound a molecular imaging tool, contrast microbubbles can be functionalized with ligands such as antibodies or peptides that bind molecular marker of interest with high affinity (Klibanov, Hughes et al. 1999). These binding ligands can either be coupled to the microbubbles using non-covalent attachment, or chemical conjugation (Klibanov 2005), or they can be integrated into the microbubble shell directly during the production process or after manufacturing (Pochon, Tardy et al. 2010; Pysz, Foygel et al. 2010).

The huge benefit of using microbubbles is that the microcirculation can be detected. Since the nonlinear signals from microbubbles occur regardless of their motion and equally when they are stationary, CE US detects the capillary bed, which is by far the largest part of the microcirculation. Of course, its spatial resolution is limited, so that individual capillaries cannot be discerned, but the microbubble content gives rise to a signal 'wash' whose intensity is proportional to the microbubble concentration and thus to the blood volume in that portion of tissue (Figure 1).

To estimate or measure perfusion, the essential tool is the transit or wash-in, wash-out curve, often referred to as the time-intensity curve (TIC) in which the time course of the transit of the microbubbles across a region of interest (ROI) is measured (Cosgrove and Lassau 2010). Two families of information are available from these TICs, those that depend on timing events, such as the arrival time and the time to peak enhancement, and those that depend on the amount of enhancement detected, such as the peak enhancement and the area under the TIC. These indices are rather more complex as they rely on a number of key assumptions. One is that the signal strength is proportional to the microbubble concentration (Blomley, Albrecht et al. 1997; Claassen, Seidel et al. 2001). Another

assumption is that all the non-linear signals in the ROI do emanate from the microbubbles, rather than from tissue.

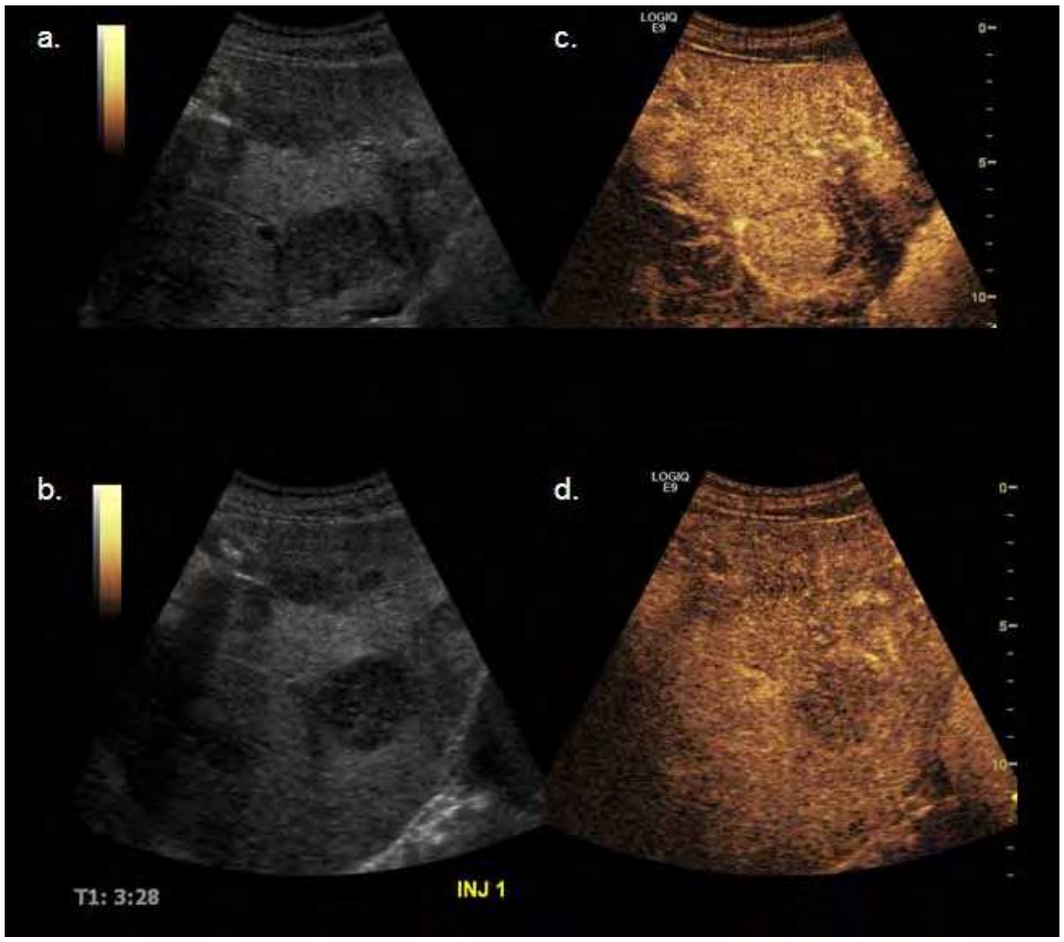

Fig. 1. Four images from a patient with pathologic proven rectal neuroendocrine tumor that is metastatic to the right lobe of the liver. (a) & (b) are conventional ultrasound images of the right lobe of the liver which demonstrates a well circumscribed, hypoechoic mass. (c) & (d) are contrast mode rapid ultrasound following injection of ~3 x 10^{-8} microbubbles that are approximately 2.5 microns in size in a volume of 2.4mL. Panels (c) and (d) demonstrate different timepoints which demonstrate enhancement of the tumor fairly homogenously in (c), and in (d) washout of the tumor with enhancement of the hepatic venous system. (Figure from Dhyani & Samir et. al. unpublished data)

The other way to generate boluses of contrast depends on the unique interaction between the imaging beam and the contrast agent: microbubbles are destroyed by higher intensity ultrasound which causes them to oscillate wildly and in complex patterns such that the gas escapes and the contrast effect is lost. The readiness with which this happens depends on the robustness of the shell, but for the commonly used clinical agent it is well within those licensed by regulatory agencies (usually a mechanical index (MI) of 1.9 is allowable). In a typical set-up, an infusion of microbubbles is used to achieve a steady blood concentration, and then a series of pulses at high MI is sent into the ROI before the system is switched back

to a low MI microbubble-specific mode for imaging (Wei, Jayaweera et al. 1998). The progressive inflow of the microbubbles in the cleared region can then be observed and the accumulation plotted. It takes the form of a rising exponential whose initial slope, β, is related to the flow rate and whose maximum value, A, is related to the equilibrium concentration of the microbubbles, also known as the fractional vascular volume. The formula that is usually deployed is:

$$R = A\ (1\text{-}e^{(-\beta t)}) \quad (1)$$

though other approximations can be used (Lucidarme, Kono et al. 2003). An important difference between ultrasound and most other contrast agents should be stressed here: because of their relatively large size, microbubbles do not diffuse across the endothelium and into the interstitial space, unlike the ionic agents used for CT and MR. Advantages of this 'destruction reperfusion' method are its ready repeatability and the clean inflow function – there is no blurring effect from the upstream circulation as occurs following an iv bolus.

The breast was one of the first tumors studies when contrast agents became available and striking differences between benign and malignant masses were reported (Kedar, Cosgrove et al. 1995). Not only was there more enhancement in malignancies but also the pattern was more chaotic. A rather crude attempt to evaluate transit times in the masses suggested that the cancers had earlier enhancement and retained the contrast for longer. Subsequent studies of breast masses have been less positive, with only poor enhancement and little differences between benign and malignant lesions as well as false positives where highly vascular fibroadenomas caused confusion (Rizzatto, Martegani et al. 2001; Jung, Jungius et al. 2005). In a more recent study of 50 consecutive patients with histological proof, QLab software was used to calculate features from TICs after bolus injections of SonoVue (Barnard, Leen et al. 2008). The area under the curve (AUC) and the peak enhancement were larger in malignant than benign lesions.

The prostate has also been studied from early after the introduction of microbubbles, both to improve detection of cancers and to assess response to antiandrogen therapy (Eckersley, Sedelaar et al. 2002). Again, the techniques were crude, exploiting what was available. More recently, microbubble-specific modes and more durable microbubbles have become available, and reports of their usefulness in targeting biopsies promise to reduce the high proportion of negative biopsies (Frauscher, Klauser et al. 2003; Wink, Frauscher et al. 2008).

A study found that DCE US was a useful method for evaluating the neovascularization of gastric carcinomas, and enhanced intensity (enhanced intensity is equal to peak intensity minus baseline intensity) had a strongly positive linear correlation with microvessel density (MVD) (Shiyan, Pintong et al. 2009). Another study found that DCE US was a valuable method for evaluating angiogenesis in colorectal tumors in vivo (Zhuang, Yang et al. 2011). This study also found that the area under the curve (AUC) had a positive linear correlation with MVD and could form a new index for assessing angiogenesis and the biological behavior of colorectal tumors. A recent study also found that the peak intensity and AUC reflected the MVD in ovarian tumors (Wang, Lv et al. 2011).

In summary, DCE US is a powerful tool for studying neovascularization and the effect of anti-angiogenic therapy, with minimal morbidity.

2.1.2 CT perfusion

CT perfusion (CTP) is a theoretical tool able to objectively quantify (with the use of mathematical models and dedicated software) the 'real' perfusion of tissues in that it only measures the density difference produced by the contribution of contrast material (and therefore of blood) to tissues. CTP is based on two indispensable technical requirements.

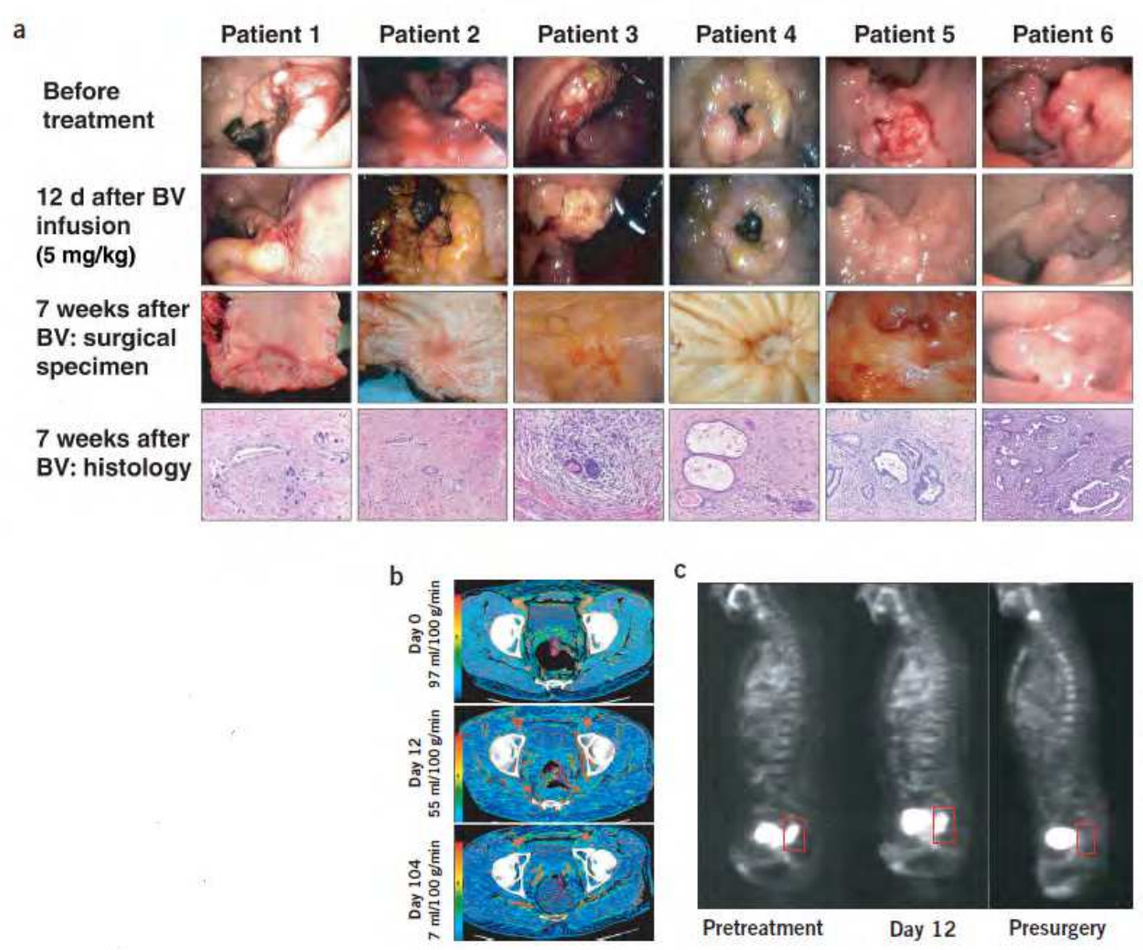

Fig. 2. Effect of treatment on tumors in patients who completed entire combined treatment regimen, and surgery. (a) Endoscopic and pathological evaluation of rectal tumors. Surgical specimens showed grade II tumor regression in patients 1-5 and grade III in patients 6, by Mandard criteria. Endoscopic image (instead of surgical specimen) was taken for patients 6, 3.5 weeks before surgery. BV, bevacizumab. (b) Representative functional CT images of blood perfusion before treatment (day 0), after bevacizumab (day 12) and after completion of treatment (day 104) in patient 5. (c) Tumor FDG uptake before treatment (pretreatment), 12d after bevacizumab treatment and 6-7 weeks after completion of all neoadjuvant therapy (presurgery). Saggital projections of FDG-PET scans for patient 1 are shown. Tumor is outlined in box, posterior to the bladder. (Reprinted with permission from Nature Medicine, 10(2), Willet et al. Direct evidence that the VEGF-specific antibody bevacizumab has antivascular effects in human rectal cancer., 145-7, Copyright 2004)

The first is the performance of repeated CT scans of the volume being analyzed (also known as dynamic, cine or perfusion scans). These need to be acquired before, during and after intravenous administration of iodinated contrast material to enable the study of density variations over time. The density measured by CT in the unit volume (voxel) is directly proportional to the quantity of contrast material present within it (Lee, Purdie et al. 2003). The contrast material contained within the tissue volume being studied is due to contrast material in vessels and contained in the extravascular/cellular space (or more simply, interstitial space) due to passive diffusion (Cenic, Nabavi et al. 2000). The second requirement is the selection of the arterial input. Placement of an ROI on an artery (arterial input) makes it possible to obtain a density/time curve, expressed in Hounsfield units (HU) per second (s), which is compared with the density/time curve of the tissues being studied, which is also obtained with placement of an ROI. Thanks to the comparison, the quantity of contrast material within vessels (vascular component) can be distinguished from contrast material within the interstitium (extravascular/cellular component). Lastly, with the use of a number of kinetic models, perfusion parameters can be calculated that quantify perfusion of the tissues being studied (Figure 2).

Two-compartment (or Patlak) analysis sees the vascular compartment and the extravascular/cellular compartment as distinct, and quantifies exchange between them (Patlak, Blasberg et al. 1983). It provides an estimate of blood volume (BV) within the microvasculature and the extraction fraction (EF), also known as the transit constant (K^{trans}), which is the sum of the flow within the microvasculature and capillary permeability. One-compartment analysis (or slope method) enables the calculation of perfusion with short-duration perfusion scans. Perfusion can be calculated as the ratio between the maximum slope of the density/time curve of tissue and the peak density reached by the artery selected as arterial input. The main advantage of this method is that it allows the calculation of perfusion with short-duration scans, in that the density/time curve of tissues reaches its maximum slope well before peak density. Short-duration scans are defined to include only the first pass of contrast material to avoid blood recirculation from interfering with perfusion quantification. In addition, they offer the advantage of being able to be performed in conditions of breath-hold in critical regions, thus limiting the possibility of motion artifacts. Nonetheless, this kinetic model is by its nature highly sensitive to noise present in the acquired images in that images are analyzed in a 'discontinuous' manner. Perfusion is, in fact, calculated by using only four images: the baseline image, the image obtained at peak density of the artery and the two subsequent images that show the greatest differences in tissue density. The presence of noise in one of these images can invalidate perfusion quantification (Miles and Griffiths 2003).

Deconvolution-based perfusion analysis applies a mathematical operation of deconvolution to compare the density/time curve obtained from the arterial input and from the tissue being studied to obtain a theoretical concentration curve (of contrast material in the tissue being studied/time), known as the residual impulse response function (IRF) (Bronikowski, Dawson et al. 1983). Using the first part of the concentration curve, it can reasonably be assumed that the contrast material lies solely within the vascular compartment. In this fashion, blood flow (BF), BV and mean transit time (MTT) of blood within the microvasculature can be calculated according to the central volume principle, whereby BF = BV/MTT. In reality, the contrast material is distributed in the vascular compartment only exclusively in the brain parenchyma (where the blood-brain barrier hinders it passage into

the extravascular/cellular component), in the testicle and in the retina. In all other organs, the contrast material spreads via capillaries into the interstitium. Nonetheless, most contrast material diffuses in the interstitium late, and the amount that diffuses during the first pass is small. It can therefore be theoretically assumed that the contrast material is only in the vascular compartment in all other parenchyma if only the early scans are used for perfusion analysis (within the first 45-60s from contrast administration), with a maximum error of 15%(Purdie, Henderson et al. 2001). Using the last part of the curve and the St. Lawrence and Lee adiabatic approximation, passage of contrast material into the interstitium can be quantified, with inclusion in the perfusion analysis of the CT scan performed after the first phase (therefore known as the interstitial phase). Calculating the permeability surface area-product (PS) is done according to the following equation:

$$PS = -BF\ [in(1-E)], \tag{2}$$

where E is the fraction of contrast that leaks into the interstitium from the vascular space (EF) (Petralia, Preda et al. 2010).

A study of 23 patients with colorectal adenocarcinoma found that tumor permeability surface-area product and blood volume correlate positively with MVD and may reflect the microvascularity of colorectal tumors (Goh, Halligan et al. 2008). A study in 6 patients with primary or locally advanced adenocarcinoma of the rectum found that after a single infusion of bevacizumab (a VEGF-specific antibody) there was a significant decrease in tumor blood flow (40-44%) and blood volume (16-39%), which was accompanied by a significant decreased in tumor MVD (Willett, Boucher et al. 2004). A study of 20 patients with resectable soft tissue sarcoma treated with neoadjuvant bevacizumab and radiotherapy found that the BV, BF and PS decreased by 62-72% (Yoon, Duda et al. 2010). A study in patients treated with antiangiogenic therapy for metastatic renal cell carcinoma found that the baseline perfusion parameters were higher in responders than in stable patients, and that after the first cycle of treatment there was a significant decrease in BF and BV in patients receiving antiangiogenic treatment. They concluded that perfusion parameters determined with DCE CT could help predict biological response to antiangiogenic drugs before beginning therapy and help detect an effect after a single cycle of treatment (Fournier, Oudard et al. 2010). A further study in patients with advanced lung adenocarcinoma found that BF, BV and permeability values were higher in responding patients than in the other patients, with a significant difference at second follow-up for BF, BV and permeability (Fraioli, Anzidei et al. 2011). A study in patients with advanced HCC treated with bevacizumab initially and then in combination with gemcitabine and oxaliplatin, found that there was a significant decrease in BF, BV, and PS and an increase in MTT from baseline. They also found that tumors with higher baseline MTT values correlated with favorable clinical outcome and had better 6 months progression-free survival. The baseline K^{trans} of responders was significantly higher than that of nonresponders. They concluded that CTP was a more sensitive image biomarker for monitoring early antiangiogenic treatment effects as well as in predicting outcome at the end of treatment and progression-free survival as compared with RECIST and tumor density (Jiang, Kambadakone et al. 2011). Another study found that perfusion MDCT can detect focal blood changes even when the tumor is shrinking, possibly indicating early reversal of tumor responsiveness to antiangiogenic therapy (Sabir, Schor-Bardach et al. 2008).

2.1.3 Dynamic contrast enhanced MRI

Functional dynamic contrast enhanced MRI (DCE-MRI) relies on the "leaky" nature of angiogenic blood vessels associated with malignancy. DCE-MRI is the acquisition of serial images before, during, and after the administration of an intravenous contrast agent, which produces time series images that enable pixel-by-pixel analysis of contrast kinetics within the tumor. PK models provide a means of summarizing contrast enhancement data in terms of parameters that relate to underlying vascular anatomy and physiology. Commonly used PK models assume that the contrast agent resides in and exchanges between two compartments in the tumor: the vascular space and the extravascular-extracellular space (EES) (Tofts 1997; Tofts, Brix et al. 1999). The contrast agent enters the tumor through the vascular space by perfusion, and diffuses between the vascular space and the EES. The rates of diffusion from the vascular space to the EES are determined by the concentrations of contrast agent in plasma and EES and the size and permeability of the capillary-EES interface (Brix, Semmler et al. 1991; Furman-Haran, Margalit et al. 1996; Knopp, Weiss et al. 1999; Tofts, Brix et al. 1999; Knopp, Giesel et al. 2001).

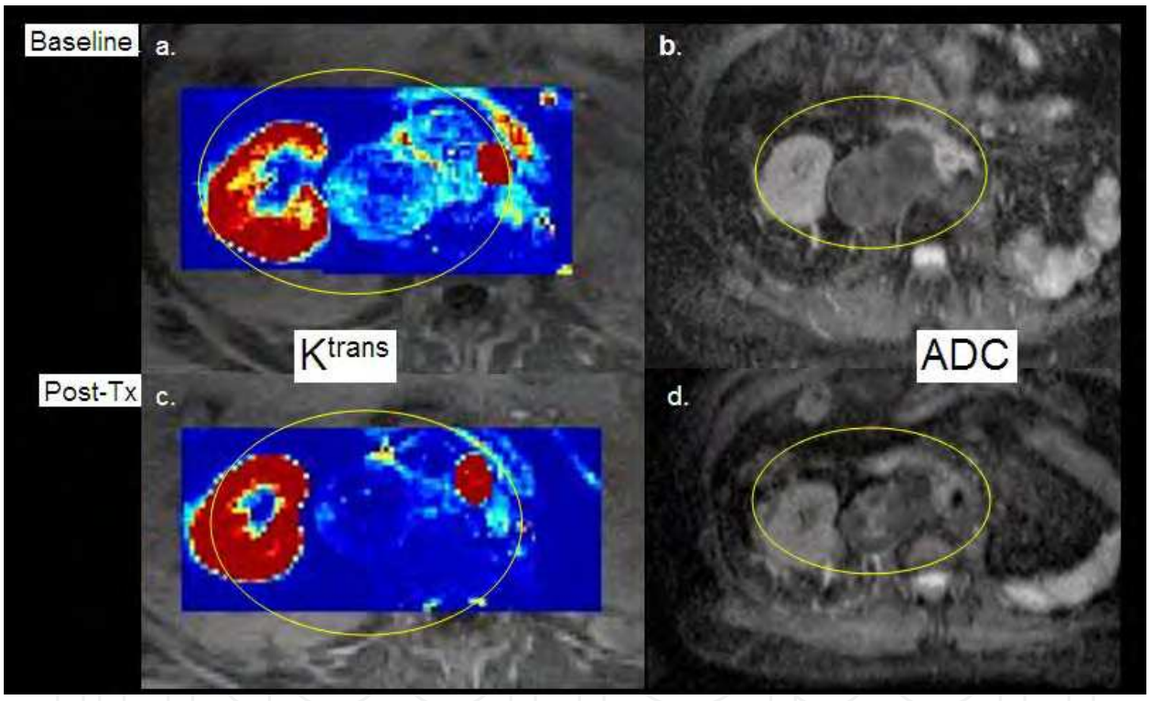

Fig. 3. Axial MR images from a patient with known metastatic renal cell carcinoma metastatic to retroperitoneal lymph nodes. (a) Overlying T1 weighted post contrast images are parametric permeability (K^{trans}) images derived from bolus injection of gadolinium DTPA mathematically derived from analysis schemes as described in section 2.1.3. Please note the increased permeability throughout the metastatic lymph node. (b) Parametric images representing the apparent diffusion coefficient (ADC) at approximately the same level. Please note the homogeneous decreased signal intensity on ADC maps throughout the metastatic lymph node. One week following sunitinib therapy, there is dramatically decreased permeability within the metastatic lymph node on the superimposed K^{trans} map (c), and there is heterogeneously increased ADC within the metastatic lymph node (d), both of which correspond to physiologic response to therapy. Figure from Rosen et al (unpublished data).

The majority of DCE-MRI studies are performed with small molecule, FDA approved Gadolinium based contrast agents. By mapping the T1 relaxation constant parametrically, and dynamically "following" the distribution of the contrast agent through the tumor microvasculature utilizing volumetric T1 weighted imaging, one can model the permeability and other parameters that may serve as surrogate biomarkers of angiogenesis (Figure 3 and 4). To do this, the change in tumor concentration with time is governed by the differential equation:

$$dC_{tumor}/dt = K^{trans}C_p - k_{ep}C_{tumor} \quad (3)$$

where C_{tumor} and C_p are the concentration of the agent in the EES and plasma space, respectively, K^{trans} is the transfer constant between the plasma and the EES, and $K_{ep} + K^{trans}/v_e$, where v_e is the fraction of tumor volume occupied by the EES. Thus the concentration of contrast agent within the tumor is determined by the blood plasma concentration curve and the two parameters, K^{trans}, the transfer constant, and the EES fractional volume index, v_e (Tofts, Brix et al. 1999).

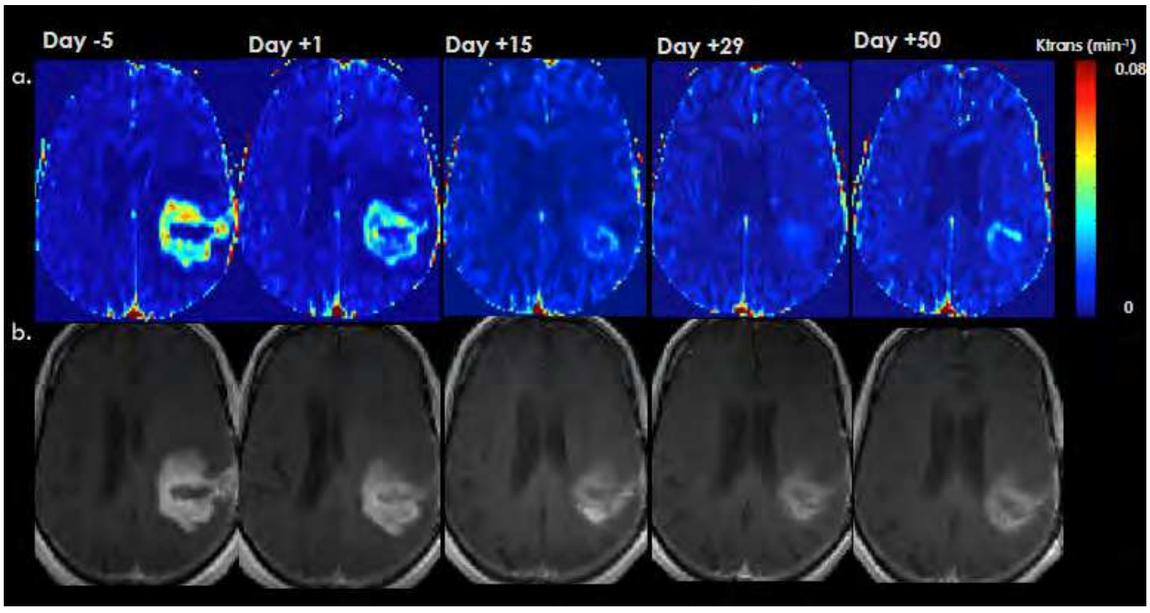

Fig. 4. (a) Maps of K^{trans}, a measure of blood-brain barrier permeability. (b) T1-weighted anatomic images after intravenous administration of a contrast agent (gadolinium-DTPA), demonstrating a region of bright signal corresponding to the recurrent brain tumor in the left frontal lobe. Note the reduction in K^{trans} following Gd-DTPA injection and kinetic analysis, and the accompanying shrinkage of the mass after injection of Cediranib (VEGF inhibitor). Figure from Jennings et. al. (unpublished data).

In relating the shape of the enhancement curve obtained from dynamic MRI studies, K^{trans} controls the height of the C_{tumor} curve and $k_{ep} = K^{trans}/v_e$ controls the shape of the curve; the smaller k_{ep}, the more delayed the enhancement. K^{trans} is a function of flow (perfusion) and permeability; the greater the flow and permeability, the greater the K^{trans} (Choyke, Dwyer et al. 2003) (Figure 5).

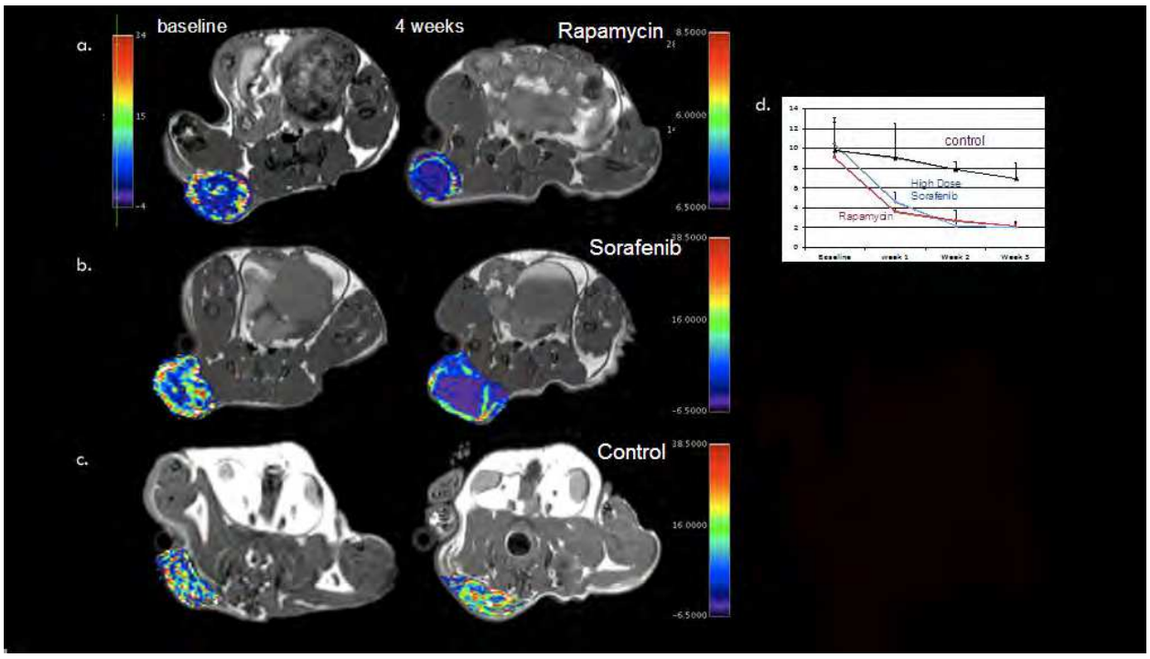

Fig. 5. T1-weighted MRI of mice with pseudocolorized VVF maps superimposed through the center of the tumor within the right flank for each treatment arm (rapamycin (a), sorafenib (b), and control (c)) at baseline and at the end of therapy. Note the heterogeneity of signal intensity and color spread throughout the cohorts at baseline, with marked decrease in vascularity in the rapamycin (a) and sorafenib (b) treated animals as compared to control (c). Of note, only 3 mice survived all 3 weeks of treatment within the rapamycin treated arm. VVF was quantified each week in each cohort and graphed (mean +/- SEM) (d). Note the parallel, rapid decrease in VVF in both the sorafenib and rapamycin treated cohorts as compared to control with a statistically significant decrease in VVF ($p<0.001$) at week 3 in both cohorts relative to control. Although there was a decrease in mean VVF in control mice, there was no statistically significant difference in VVF comparing week 3 to baseline measurements in control mice. Figure from Guimaraes et. al. (unpublished data).

Utilizing this approach in humans suffering from breast cancer, Hulka et al demonstrated a sensitivity of 86% and specificity of 93% for the diagnosis of malignancy (Hulka, Smith et al. 1995; Hulka, Edmister et al. 1997; Tofts, Brix et al. 1999). Knopp et al expanded on these results and were able to demonstrate, by correlative analysis with VEGF and CD31 analysis, significantly faster enhancement characteristics between histologic subtypes (invasive ductal carcinoma, invasive lobular carcinoma and ductal carcinoma in situ)(Knopp, Weiss et al. 1999). Subsequently, various groups have demonstrated, in vivo, in animal models and clinical trials, statistically significant differences in permeability transfer constants following

the administration of angiogenesis inhibitors (Pham, Roberts et al. 1998; Morgan, Thomas et al. 2003). Morgan et al demonstrated a rapid reduction in enhancement within 26 to 33 hours after the first dose of the VEGF inhibitor PTK 787/ZK 222584 in a liver metastasis from colorectal carcinoma. This substantial reduction in enhancement is evident across all dose groups on day 2, with a mean reduction in permeability transfer constant of 43% (Morgan, Thomas et al. 2003).

Despite these sophisticated models and encouraging results, pharmacokinetics modeling has been utilized with varying success to calculate blood volume of fractional plasma volume, with reported values demonstrating a correlation coefficient of R^2 0.61, and most studies indicate high sensitivity (>90%), but wide variability in specificity, with published values as low as 30% (Piccoli 1997). This variability is demonstrated well in a study by Su et al who performed DCE MRI on 105 patients with breast cancer and correlated it to VEGF serum marker levels as well as microvascular density as assessed post CD31 staining. Although patients with increased VEGF demonstrated higher CD31 microvascular densities, no significant association between MRI parameters and these other surrogate markers was demonstrated (Su, Cheung et al. 2003). In a study of 38 patients with advanced hepatocellular carcinoma treated with sunitinib, the investigators found significant decreases in K^{trans} and K_{ep} to approximately half. Moreover, the extent of decrease in K^{trans} in patients who experienced partial response/stable disease was significantly greater (two-fold on average) compared with patients with progressive disease or who died during the first two cycles of therapy (Zhu, Sahani et al. 2009).

DCE-MRI, in summary, has exciting potential to study the early effects of anti-angiogenic therapy in various organ systems.

2.1.4 Positron emission tomography

PET has been used in some studies to assess tumor blood flow with $H_2\,^{15}O$ as a biological endpoint of response to antiangiogenic agents (Herbst, Mullani et al. 2002). The principal advantage of $H_2\,^{15}O$ is that it is a 'freely diffusible' tracer, meaning that its uptake by the tumor is not limited by vascular permeability. $H_2\,^{15}O$ PET has been used to measure blood flow in several tumor types, including breast (Beaney, Lammertsma et al. 1984) and brain tumors (Ito, Lammertsma et al. 1982). The first report of the use of PET to measure vascular pharmacodynamics in humans was part of a phase 1 dose-escalation study of the tumor vascular targeting agent combretastatin A4 phosphate (CA4P) (Anderson, Yap et al. 2003). $H_2\,^{15}O$ PET was used to measure tumor and normal tissue perfusion and blood volume, before and after the administration of CA4P. Significant reductions in tumor perfusion were measured 30 minutes after administration of CA4P. However, there are potential limitations. $H_2\,^{15}O$ has a short half-life (2 minutes) and therefore studies require an on-site cyclotron and a separate tracer synthesis for each injection. In small tumors, partial volume effects may be significant if the tumor size is less than twice the resolution of the scanner. Second, there is a phenomenon known as 'spill over' or 'spill in' of counts from surrounding structures with high blood flow, such as the heart and the aorta, or within areas of relatively high blood flow, such as the liver, therefore limiting the use of this technique in the lung, liver and mediastinum.

2.2 Steady state blood volume determinations of neovascular density

2.2.1 Magnetic resonance imaging

Ultrasmall super paramagnetic iron oxide (a.k.a. magnetic nanoparticle (MNP)) is a steady state blood pool agent that creates contrast through magnetic susceptibility variations proximal to the vascular network (Enochs, Harsh et al. 1999; Tropres, Grimault et al. 2001; Corot, Robert et al. 2006; Persigehl, Bieker et al. 2007), which results in changes in inherent and induced transverse relaxation times defined as T_2 and T_2*, respectively. Accurate evaluation of R_2* ($1/T_2$*) or R_2 ($1/T_2$) necessitate defining two or more points on the natural or induced transverse relaxation decay curve. Addition of contrast agent increases R_2* ($1/T_2$*) thus causing limits on sampling as the T_2* is shortened. It can be shown that:

$$\Delta R_2^* \text{ or } \Delta R_2 \propto \log [S^{post}/S^{pre}] \quad (4)$$

where, S^{pre} and S^{post} are pre- and post-contrast MRI signal intensity (Brown and Giaccia 1998). The change in transverse relaxation rate ΔR_2 ($1/\Delta T_2$) and changes in effective transverse relaxation rate ΔR_2* ($1/\Delta T_2$*) caused by the contrast agent are proportional to tumor blood volume (BV) fraction (Belliveau, Rosen et al. 1990; Dennie, Mandeville et al. 1998; Ostergaard, Smith et al. 1998). Therefore, the capability of MNP to modulate the effective transverse relaxation rate, R_2*, is exploited where the difference of R_2* before and after administration of MNP will be useful in determining microvessel density (Hyodo, Chandramouli et al. 2009).

Bremer et al first utilized intravital microscopy to determine whether a prototype magnetic nanoparticle (MION) agent truly had intravascular distribution in tumor microenvironment (Bremer, Mustafa et al. 2003). For these experiments a green fluorescent protein expressing 9L tumor model was utilized, in which tumor microvasculature is clearly outlined against fluorescent tumor cells, even at very high spatial resolution, which demonstrated that MION selectively enhanced the vascularity without any significant leakage into tumor interstitium during time of observation (30 minutes). They also found that steady state measures of vascular volume fraction (VVF) with MRI allow a volumetric, in vivo, non-invasive assay of microvascular density in experimental tumor models.

Pancreatic adenocarcinoma xenograft lines were subcutaneously implanted into nude mice, which were then therapies targeted to 3 loci of the sonic hedgehog signaling pathway. MRI imaging was performed 1 week after therapy, pre and post injection of MION-47. Following treatment, tumors showed a significant decrease in VVF compared to controls (Guimaraes, Rakhlin et al. 2008). A study on fibrosarcoma-bearing nude mice which were injection with a thrombogenic vascular targeting agent (VTA) found that the ΔR2* values were significantly reduced shortly after treatment initiation and concluded that USPIO-enhanced MR imaging enable early monitoring of antiangiogenic treatment of tumors (Persigehl, Bieker et al. 2007).

A recently published study on rhabdomyosarcoma-bearing mice treated with bevacizumab or saline as control, found that multiecho ΔR2* MR relaxometry allowed an early and quantitative assessment of tumor vascularization changes in response to an antiangiogenic treatment (Ring, Persigehl et al. 2011). Another study on renal cell carcinoma-bearing mice treated with rapamycin (mTOR inhibitor), sorafenib (VEGF inhibitor) or saline control, VVF correlated with MVD and that the VVF in all treatment arms differed from control and

declined weekly with treatment. They also reported that VVF changes with rapamycin were similar to high-dose sorafenib (Guimaraes, Ross et al. 2011).

Although not FDA approved, MNP enhanced MRI measures allow for interrogation of altered tumor microvascular morphology, and may serve as a robust means of evaluating the microstructural microvascular changes associated with anti-angiogenic therapy in humans.

2.3 Specific molecular markers of angiogenesis

Advances in knowledge of tumor angiogenesis have resulted in the identification of several molecules in tumor angiogenic signaling. These molecules have been exploited for their use as targets for molecular imaging and quantification of tumor angiogenesis. Furthermore, discovery of these molecules has led to realization of the concept that tumor vessels can be selectively targeted for therapy. Non-invasive molecular imaging of tumor angiogenesis can allow for much easier diagnosis and better prognosis of cancer, as well as more accurate treatment monitoring, which will eventually lead to personalized molecular medicine.

2.3.1 Vascular endothelial growth factor

Vascular endothelial growth factor (VEGF) is one of the key factors regulating angiogenesis. Most of the vasculogenic and angiogenic effects of VEGF are mediated through two endothelium-specific receptor tyrosine kinases, VEGF receptor 1 (VEGFR-1) and VEGF receptor 2 (VEGFR-2)(Millauer, Wizigmann-Voos et al. 1993). VEGFR-1 is critical for physiologic and developmental angiogenesis, and VEGFR-2 is the major mediator of the mitogenic, angiogenic, and permeability-enhancing effects of VEGF (Ferrara 2004). In the imaging studies reported to date, however, specificity for ether VEGFR-1 or VEGFR-2 has rarely been achieved, because most of the tracers are based on $VEGF_A$ isoforms, which bind to both VEGFRs. Because of a high level of VEGFR-1 expression, rodent kidneys can take up a significant amount of a $VEGF_A$-based tracer, a fact that often makes the kidneys the dose-limiting organ. Because VEGFR-2 is generally accepted to be more functionally important than VEGFR-1 in cancer progression, this limits the use of current techniques.

Recently, in vivo CE US imaging of VEGF/VEGFR expression has been reported. In 2 murine tumor models, microbubbles conjugated to anti-VEGFR-2 monoclonal antibodies were used to image VEGFR-2 expression (Willmann, Paulmurugan et al. 2008). The targeted microbubbles produced a significantly higher average signal intensity than control microbubbles, and the signal intensity was significantly lower when anti-VEGFR-2 antibodies (blocking antibodies) were used, demonstrating target specificity.

^{99m}Tc-labelled human $VEGF_{121}$ (one of the homodimeric isoforms of $VEGFR_A$) has been used as a molecular imaging marker of VEGFR expression in an orthotopic mouse model of mammary adenocarcinoma, and for the imaging of tumor vasculature before and after tumoricidal cyclophosphamide treatment (Blankenberg, Backer et al. 2006). [^{123}I]$VEGF_{165}$ has also been reported as a potential tumor marker (Cornelissen, Oltenfreiter et al. 2005), but despite the high receptor affinity of this tracer, biodistribution in melanoma tumor-bearing mice indicated poor tumor-to-background ratios, most likely due to the low metabolic stability (deiodination) of the compound. Nonetheless, biodistribution, safety, and absorbed

dose of [^{123}I]VEGF$_{165}$ was studied in patients with pancreatic carcinoma (Li, Peck-Radosavljevic et al. 2004). Following IV administration, sequential images were recorded during the initial 30 minutes after injection. Although a majority of primary pancreatic tumors and their metastases were visualized by the [^{123}I]VEGF$_{165}$ scan, the organ with the highest absorbed dose was the thyroid, indicating severe deiodination of the probe.

To target the VEGFR-2, Backer et al (Backer, Patel et al. 2006) used single chain VEGF (scVEGF) with an N-terminal cysteine-containing tag (Cys-tag), which can be used for site specific attachment of various agents (Backer, Levashova et al. 2008). The scVEGF-based family of probes has been validated to target the VEGF receptor in vitro and in vivo tumor angiogenesis (Blankenberg, Backer et al. 2006; Levashova, Backer et al. 2008)

^{64}Cu-labelled VEGF$_{121}$ has been used for PET imaging of tumor angiogenesis and VEGFR expression (Cai, Chen et al. 2006). DOTA-VEGF$_{121}$ (where DOTA denotes 1,4,7,10-tetraazacyclododecane-1,4,7,10-tetraacetic acid) exhibits nanomolar receptor affinity in vitro. In an animal model, microPET imaging revealed rapid, specific, and prominent uptake of [^{64}Cu]DOTA-VEGF$_{121}$ in highly vascularized small xenografts (high VEGFR-2 expression) but significantly lower and sporadic uptake in large tumors (low VEGFR-2 expression). Substantial tracer uptake in the kidneys was also observed, most likely due to the high VEGFR-1 expression in this organ.

A VEGFR-2-specific PET tracer based on mutant VEGF$_{121}$ has been recently developed (Wang, Cai et al. 2007). The D63AE64AE67A mutant of VEGF$_{121}$ (VEGF$_{DEE}$), compared with VEGF$_{121}$ had an affinity for binding to VEGFR-1 that was 20-fold lower, without a significant reduction in VEGFR-2-binding affinity.

HuMV833, a humanized mouse monoclonal anti-VEGF antibody was labeled with ^{124}I for PET imaging of solid tumors in phase 1 trial cancer patients (Jayson, Zweit et al. 2002). Antibody distribution and clearance were markedly heterogeneous between and within patients and between and within individual tumors, suggesting that dose escalation design of phase 1 studies with antiangiogenic antibodies such as HuMV833 would be problematic.

2.3.2 Integrins

Integrins are a family of cell adhesion molecules consisting of two noncovalently bound transmembrane subunits (α and β) that pair to create heterodimers with distinct adhesive capabilities. Integrin $\alpha_v\beta_3$ mediates the migration of endothelial cells through the basement membrane during blood-vessel formation (Josephs, Spicer et al. 2009). Imaging of integrin $\alpha_v\beta_3$ expression is promising for the assessment of angiogenesis, as integrin $\alpha_v\beta_3$ is significantly up-regulated on endothelium during angiogenesis, but not an quiescent endothelium (Brooks, Clark et al. 1994). In addition, in healthy tissue, expression of integrin $\alpha_v\beta_3$ is highly restricted with significant amounts only observed in osteoclasts (van der Flier and Sonnenberg 2001). Integrin $\alpha_v\beta_3$, which mediates the migration of endothelial cells through the basement membrane during blood-vessel formation, binds to peptides containing the amino-acid sequence arginine-glycine-aspartic acid (RGD) within the interstitial matrix (Haubner 2006). By labeling these peptides with ^{125}I, ^{111}In, ^{64}Cu, ^{99m}Tc, ^{18}F or fluorescence dyes, specific binding of imaging agents to integrin $\alpha_v\beta_3$ in tumors has been demonstrated (Haubner, Wester et al. 1999; van Hagen, Breeman et al. 2000; Haubner,

Wester et al. 2001; Janssen, Oyen et al. 2002; Chen, Conti et al. 2004; Beer, Lorenzen et al. 2008).

Targeted ultrasound imaging of integrin $\alpha_v\beta_3$ during tumor angiogenesis has been reported (Ellegala, Leong-Poi et al. 2003). In a rat model of human glioblastoma, CEU was performed with microbubbles coated with echistatin, an RGD-containing disintegrin, which binds specifically to integrin $\alpha_v\beta_3$. The CEU signal was found to be highest at the periphery of tumors, where integrin expression was most prominent as indicated by immunohistochemistry, and correlated well with tumor microvascular blood volume.

Gd3+-containing paramagnetic liposomes (300-350nm in diameter) have been used for MRI of integrin $\alpha_v\beta_3$ expression (Sipkins, Cheresh et al. 1998). In that study, mMRI of squamous cell carcinomas in a rabbit model was achieved with LM609, a mouse antihuman integrin $\alpha_v\beta_3$ monoclonal antibody, as the targeting ligand. Peptidomimetic integrin $\alpha_v\beta_3$ antagonist-conjugated magnetic magnetic nanoparticles were tested in a Vx-2 squamous cell carcinoma model with the common clinical field strength of 1.5 T(Winter, Caruthers et al. 2003). The targeted nanoparticles increased the MR signal dramatically in the periphery of the tumor at 2 hours after injection. Despite their relatively large size (~270nm in diameter), these nanoparticles penetrated into the leaky tumor neovasculature but did not migrate into the interstitum in appreciable amounts. In a later report, athymic nude mice bearing human melanoma tumors were successfully imaged with systemically injected integrin $\alpha_v\beta_3$-targeted paramagnetic nanoparticles (Schmieder, Winter et al. 2005). Very small regions (about 30mm^3) of angiogenesis associated with nascent melanoma tumors were visualized by this technique, which may enable phenotyping and staging of early melanomas in clinical settings.

Integrin $\alpha_v\beta_3$-targeted ultrasmall SPIO nanoparticles were used with a 1.5T RI scanner for the noninvasive differenciation of tumors with large and small fractions of integrin $\alpha_v\beta_3$–positive tumor vessels (Zhang, Jugold et al. 2007). After injection of RGD peptide-conjugated small SPIO nanoparticles, T2*-weighted MR images revealed the heterogeneous distribution of integrin –positive tumor vessels, as evidenced by an irregular signal intensity decrease. In contrast, the signal intensity decreased homogeneously in the control tumor, with predominantly small and uniformly distributed vessels.

In recent years, many fluorescently labeled cyclic RGD peptides have been developed for near infrared fluorescence imaging like RGD-Cy7, RGD-Cy5.5, RGD-QD705 (Chen, Conti et al. 2004; Cai, Shin et al. 2006; Wu, Cai et al. 2006) and cyclic RGD coupled to IRDye 800CW-labeled peptide which is even more shifted towards the infrared parts of the spectrum resulting in ideal fluorescent characteristics for in vivo use (Adams, Ke et al. 2007). Mulder et al (Mulder, Koole et al. 2006; Mulder, Castermans et al. 2009) recently described paramagnetic lipid-encapsulated quantum dots with RGD presented at the outside and a green fluorescent quantum dot at the inside of the micellar shell. These targeted particles are both suitable for fluorescence imaging as well as MRI, thus providing unique opportunities for the use of multimodality molecular imaging.

Several groups have improved $\alpha_v\beta_3$ integrin specificity, binding affinity, and possible targeted delivery of therapeutics, by coupling multiple RGD motifs on a backbone molecule (Kok, Schraa et al. 2002; Cheng, Wu et al. 2005; Mulder, Koole et al. 2006; Jin, Josserand et al.

2007; Mulder, Castermans et al. 2009). Although, many types of tumor cells are positive for $\alpha_v\beta_3$ integrin, RGD-modified proteins mainly localize at the tumor endothelium and not in the tumor itself (Schraa, Kok et al. 2002).

The commercially available near infrared fluorescent (NIRF) probe IntegriSense (Visen Medical) consists of a small molecule nonpeptide $\alpha_v\beta_3$ antangonist fused to the VivoTg-S680 near infrared fluorophore. IntegriSense has a much higher specificity for $\alpha_v\beta_3$ integrin compared to RGD-based probes. Unlike RGD-based probes, extravasation of IntegriSense does occur and the probe localizes at both the surface of $\alpha_v\beta_3$ integrin positive endothelial cells and the surface $\alpha_v\beta_3$ integrin positive tumor cells. Furthermore, IntegriSense is internalized by the $\alpha_v\beta_3$ integrin positive tumor cells leading to a slower clearance of the probe from tumors compared to the surrounding tissues. A drawback of the slower clearance from the tumor is the practical upper limit on the possible frequency of repeated measurements (Kossodo, Pickarski et al. 2010).

A dimeric RGD peptide $E[c(RGDyK)]_2$ (abbreviated as FRGD2) has been labeled with ^{18}F. A high accumulation of ^{18}F-FRGD2 in integrin $\alpha_v\beta_3$ –rich tumors was demonstrated with a high tumor/background ratio at late time points of imaging (Zhang, Xiong et al. 2006). A glycopeptides based on c(RGDyK) was later labeled with 18F and the resulting 18F-galacto-RGD was found to be safely administered to patients and allowed detection of integrin-positive tumors (Haubner, Weber et al. 2005). Despite the successful translation of 18F-galacto-RGD into clinical trials however, several key issues remain to be resolved, such as tumor-targeting efficacy, pharmacokinetics, and the ability to quantify integrin $\alpha_v\beta_3$ density in vivo. Indeed, other promising multimetric RDG peptides are being investigated and may give better localization than galacto-RGD (Cai, Niu et al. 2008)

Etaracizumab, a humanized murine monoclonal antibody against human integrin $\alpha_v\beta_3$ has been conjugated with a chelating agent DOTA and labeled with ^{64}Cu. The resulting [^{64}Cu]DOTA-etaracizumab correlated well with integrin $\alpha_v\beta_3$ in tumor xenografts via PET imaging (Cai, Wu et al. 2006). MicroPET studies revealed avid [^{64}Cu]DOTA-etaracizumab uptake in integrin $\alpha_v\beta_3$ -positive tumors. The receptor specificity of [^{64}Cu]DOTA-etaracizumab was confirmed by effective blocking of tumor uptake with co-administration of non-radioactive etaracizumab.

A nanoparticle-based probe has been used for both MRI and optical imaging of integrin $\alpha_v\beta_3$. MRI-detectable and fluorescent liposomes carrying RGD peptides were evaluated for in vivo tumor imaging (Mulder, Strijkers et al. 2005). Both RGD-conjugated liposomes and RAD (a control peptide that does not bind to integrin $\alpha_v\beta_3$)-conjugated liposomes provided enhanced T1-weighted MR contrast. Ex vivo fluorescence microscopy revealed that RGD-conjugated liposomes were specifically associated with the activated tumor endothelium, whereas RAD-conjugated liposomes were located in the extravascular compartment.

A quantum dot (QD)-based probe for NIRF imaging and PET of integrin $\alpha_v\beta_3$ has been developed (Cai, Chen et al. 2007). QD surface modification with RGD peptides allowed for integrin $\alpha_v\beta_3$ targeting, and DTA conjugation enabled PET after ^{64}Cu labeling. It was found that the majority of the probe in the tumor was within the vasculature, as evidenced by excellent overlay of the QD fluorescence signal and vasculature integrin $\alpha_v\beta_3$ staining. This

dual-modality (PET/NIRF imaging) probe can confer sufficient tumor contrast at a concentration much lower than that required for in vivo NIRF imaging, significantly reduces the potential toxicity of cadmium-based QDs, and may hasten the future translation of QD-based imaging agents to clinical and biomedical applications.

2.3.3 Transforming growth factor β

Transforming growth factor β (TGF-β) signaling plays a role in several biological processes, including embryonic development, carcinogenesis, wound healing, and angiogenesis (Bernabeu, Lopez-Novoa et al. 2009). In normal cells, the TGF-β pathway restricts cell growth, differentiation and cell death. In contrast, in malignant cells, various components of the TGF-β signaling pathway become mutated thereby exploiting the ability of TGF-β to modulate growth promoting processes, including cell invasion and angiogenesis. TGF-β signaling is mediated by TGF-β binding to TGF-β receptors, of which, there are three classes: Type I and II are heterodimeric receptor whereas type III are homodimeric receptors . CD105, also known as endoglin, is a TGF-β type III receptor that has been shown to participate in signaling angiogenesis. Endoglin is predominantly expressed on proliferating endothelial cells (Fonsatti, Altomonte et al. 2003), and inhibition of its expression has been shown to restore the growth suppressing signals of the TGF-β signaling pathway (Ma, Labinaz et al. 2000). Thus, endoglin is an attractive molecular target of angiogenesis since it is over-expressed on tumor-associated endothelium (Bernabeu, Lopez-Novoa et al. 2009).

Avidin (Av) was incorporated into the shell of perfluorocarbon-exposed sonicated dextrose albumin micobubbles (Av-MBs) to anchor biotinylated monoclonal antibodies (mAbs) (Korpanty, Grayburn et al. 2005). A rat anti-mouse CD105 mAb (MJ7/18) and an isotype-matched control mAb were investigated for biotinylation, microbubbles incorporation, and cellular studies. It was found that MJ7/18-conjugated microbubbles bound specifically to endothelial cells but not fibroblasts, while the control mAb-conjugated Av-MBs did not exhibit CD105-specific targeting. After demonstrating the proof-of-principle, a follow-up study was carried out to follow the vascular response of therapy in mouse models of subcutaneous and orthotopic pancreatic adenocarcinoma (Korpanty, Carbon et al. 2007). For comprehensive investigation of angiogenesis in tumor-bearing mice treated with anti-VEGF mAbs and/or gemcitabine (a nucleoside analog with known activity against pancreatic adenocarcinoma), the localization of microbubbles targeting CD105, VEGFR-2, or VEGF-activated blood vessels 9the VEGF-VEGFR complex) was monitored by ultrasound (Di Marco, Di Cicilia et al. 2010). In the subcutaneous model, receptor-targeted microbubbles gave significantly better enhancement of tumor vasculature than the non-targeted or control mAbs-conjugated microbubbles. In addition, video intensity from targeted microbubbles correlated with the level of target expression (CD105, VEGFR-2, or the VEGF-VEGFR complex), as well as with MVD in tumors under either anti-angiogenesis or cytotoxic therapy.

One study investigated the applicability of a human umbilical vein endothelial cell (HUVEC)-based in vitro model to mimic physiological and angiogenic vasculature (Vag, Schramm et al. 2009). High fluorescence signal was observed in proliferating HUVECs due to CD105 expression.

Molecular MRI of CD105 expression in tumor-bearing rats was achieved with Gd-DTPA-containing stabilized liposomes (Gd-SLs) (Zhang, Feng et al. 2009). A series of targeted and non-targeted MRI contrast agents were compared in glioma-bearing rats: Gd-DTPA, Gd-SLs, Gd-SLs conjugated to anti-CD105 mAbs (CD105-Gd-SLs), and Gd-SLs conjugated to control mAbs (IgG-Gd-SLs). Serial T1-weighted MRI before and after contrast agent administration revealed that the area with enhanced MRI contrast was restricted for CD105-Gd-SLs but not for the other three groups. In addition, the degree of contrast enhancement over time also varied between different groups. For example, Gd-DTPA gave an early contrast enhancement which peaked at 30 minutes and declined to baseline values at 60 minutes, while the signal intensity for CD105-Gd-SLs continued to increase over a period of 120 minutes. The signal intensity of IgG-Gd-SLs and Gd-SLs both peaked at 60 minutes followed by a decline, yet the rate of decrease was quite different. Ex vivo histology further revealed that the enhancement in the CD105-Gd-SLs group resulted mainly from new microvessels. However, both mature microvessels and new microvasculature were responsible for contrast enhancement in the other three groups.

A study investigated an ^{111}In-labeled anti-CD105 mAb (MJ7/18) and compared its neovascular binding, tumor accumulation, and in vivo behavior in an isotype-matched control mAb (Bredlow, Lewin et al 2000) In a B16 melanoma model, the tumors in animals receiving 111In-labelled MJ7/18 were more easily identified than animals receiving the radiolabeled control mAb. However, the tumor contrast was only modest. Ex vivo autoradiography and histology experiments of the tumor sections corroborated the different patterns of in vivo tumoral accumulation for the two antibodies. MJ7/18 exhibited intense activity in the peripheral region of the tumor, where the highest concentration of vessels was found, and much lower activity in the tumor center. On the other hand, little accumulation of activity could be found in tumors of mice that had been injected with ^{111}In-labeled control mAb.

Another study tested a ^{125}I-labeled anti-CD105 mAb (MAEND3) in a canine mammary carcinoma model (Fonsatti, Jekunen et al. 2000). After demonstrating differential expression of CD105 on human breast cancer and endothelial cells, two dogs with spontaneous mammary tumors were intravenously injected with ^{125}I-laveled MAEND3 and imaged eight hours later. Rapid and intense uptake of the radiolabeled mAb with excellent tumor-to-background ratio was observed in the tumor areas of both dogs, which were confirmed as ductal mammary adenocarcinoma after surgical excision ten days later. Another study also explored the use of ^{125}I-labeled anti-CD105 mAb for radioimmunotherapy applications in mouse tumor models (Tabata, Kondo et al. 1999). Significant growth suppression of the tumors was observed while a ^{125}I-labeled control mAb did not show any significant anti-tumor efficacy.

A ^{99m}Tc-labelled anti-CD105 mAb (E9) was investigated in freshly excised kidneys from renal carcinoma patients (Costello, Li et al. 2004). After perfusion of ^{99m}Tc-E9 through the renal artery, immunoscintigraphy revealed the presence of well-defined radioactive hot spots, which matched the positions of the tumors as identified by pre-surgery MRI and subsequent histology. Gamma-counting revealed that the median values of radioactivity uptake per gram of wet weight were > 10 fold higher in the tumors than in normal kidney tissues. Not only was CD105 specificity of the tracer confirmed by blocking studies,

immunoscintigraphy with ^{99m}Tc-E9 was also able to identify tumors that were not detected during pre-surgery MRI.

2.3.4 Matrix metalloprotienases

Expression of matrix metalloproteinases (MMPs) is associated with the removal of the extracellular matrix (ECM) barrier to allow cancer cells ad endothelial cells to invade the basement membrane. A number of MMPs are also specifically involved in angiogenesis, including MMPs 1, 2, 3, 9, and 14 (Stollman, Ruers et al. 2009).

One approach for monitoring MMP activity in tumor-bearing animal models is the use of 'smart' fluorescence probes that are bound to a synthetic graft copolymer consisting of a cleavable backbone that can act as an MMP substrate. When placed in close proximity, these polymeric fluorochromes quench each other and are not detectable. On enzymatic cleavage of the backbone by MMPs, the fluorochromes are spatially dissociated and begin to fluoresce (Bremer, Bredow et al. 2001)

3. Clinical relevance of the finding

The development of anti-angiogenic agents has been rapid to date. Although demonstrating provocative physiologic effects, the results to date have not demonstrated any significant improvements in patient outcome. This may be a result of various factors including a better understanding of the timing associated with the greatest changes occurring physiologically or morphologically within the microvasculature, a better understanding of whether the hypothesis of vascular normalization (Jain 2001; Jain 2005) (Goel, Duda et al. 2011) has bearing and may be a window into the introduction of other targeted cytotoxic agents, and improved, translatable targeted molecular imaging approaches to interrogating the tumor microenvironment. As these methods evolve in parallel, one may see come to fruition a true clinical benefit to the outstanding insight proposed from Dr. Folkman's (Folkman 1971) seminal article many years ago.

4. View to the future

In order to bridge this gap in understanding the effects of angiogenesis, significant improvements and developments will have to occur within the following areas: 1) improvements in quality assurance and quality control associated with the physiologic measurements on interrogate the permeability, blood flow, and blood volume values that MRI, CT and PET; 2) improvements in targeted, molecular imaging approaches that may reflect the molecular changes that are occurring following administration of extant and novel anti-angiogenic or vascular disrupting agents, and lastly; 3) utilizing both of these approaches to better investigate and have a more comprehensive understanding of the validity and regulation of vascular normalization as a hypothesis for improved chemotherapeutic delivery is crucial.

Perfusion imaging with MRI, CT or PET provides a unique window into the vascular morphology and physiologic changes associated with agents that disrupt the tumor microenvironment or microvasculature. As we have noted in this chapter thus far, these have had a profound impact on the initial evaluation of agents that target the tumor microvasculature. If performed with proper quality assurance/quality control, and critical

understanding of baseline variance, measures will allow for a more robust understanding of the true effects of agents targeted to the tumor microvasculature. Although many studies have demonstrated that there is in general good concordance with preclinical data and with other angiogenesis biomarkers, and if studies are performed well, the observations gleaned from these studies might improve the biologic understanding of the mechanism of drug action, potential drug interactions, and the duration of effects, however, the high variance demonstrated in many of these studies (>20% in some instances), makes proper determination of biologic effect sometimes suspect. This fact becomes more important as we go forward trying to study the correlation of these physiologic changes with clinical outcomes and relevant serum biomarkers.

MRI molecular imaging may play a role in improving some of these problems illustrated above. As noninvasive molecular imaging methods evolve, there will be an increasing possibility to personalization of therapy. For instance, imaging of MRI reporter-labeled stem cells or endothelial progenitor cells will provide new insights into their role in tumor angiogenesis, as these cell types have been implicated in tumor vascularization and potential poor response to antiangiogenic therapies (Monzani and La Porta 2008) (van der Schaft, Seftor et al. 2004). Exciting developments have been made in identification of tumor vascular specific receptors, which opens up possibilities for imaging but also monitoring using nanodevices the delivery of therapeutic agents, or gene delivery. Likewise, similar advances have been made in siRNA technology, where image-guided delivery to tumor microvasculature, visualization of this delivery via liposome technology or other nanocarriers, and detection of a therapeutic response are well within the realm of current imaging capabilities (Pathak, Penet et al. 2010). Yet, these technologies to this point remain preclinical and successful translation to the clinic remains a hurdle.

With all of the advances in imaging technology demonstrating effects and possible benefits of antiangiogenic therapy, the future of this kind of work remains unclear. One concept that has come to the fore and deserves mention is that of vascular normalization. A concept introduced by Rakesh Jain (Izumi, Xu et al. 2002), which describes the morphologic and physiologic changes that occur to tumor microvasculature accompanying anti-angiogenic therapy. This factor may be key in modulating the proangiogenic and anti-angiogenic forces ongoing in maintenance of the tumor microenvironment in addition to providing key insights into potential temporal windows for the introduction of cytotoxic agents. These questions remain the key to further improvements in the delivery of chemotherapeutic agents. "As a result, the presence and timing of therapy-induced normalization must be carefully studied in a range of human tumors, and novel therapeutics are needed. This will in part be informed by preclinical work, and also by development and validation of noninvasive biomarkers that survey the normalization phenotype. Only then will treatment be applied in a rational and judicious fashion with the intent of maximizing therapeutic outcomes" (Goel, Duda et al. 2011).

5. Take home message

The studies and techniques described attest to the validity of these extant and novel imaging techniques to probe the microstructural and morphologic microvascular changes that occur both as a result of tumor angiogenesis, and more importantly, soon after the delivery of anti-angiogenic therapy. These can be performed indirectly, by measuring hemodynamic

parameters associated and related to blood volume, permeability and blood flow through imaging. These measures have been indispensible in the rapid and noninvasive interrogation of the microvascular changes accompanying antiangiogenic therapy. As existing techniques (e.g. DCE-MRI, CT perfusion, DCE-US) become more refined and validated by multi-institutional trials, the associated biomarkers may play a more pro-active role in the personalized approach that oncology is likely to engender. Furthermore, with the recent development of novel hybrid MRI PET devices, the realization and translation of more novel, targeted imaging approaches that probe the altered signaling pathways associated with angiogenesis, may become a reality in humans.

6. References

Adams, K. E., Ke, S., Kwon, S., Liang, F., Fan, Z., Lu, Y., Hirschi, K., Mawad, M. E., Barry, M. A., & Sevick-Muraca, E. M. (2007). "Comparison of visible and near-infrared wavelength-excitable fluorescent dyes for molecular imaging of cancer." *Journal of biomedical optics* 12(2): 024017, 1083-3668

Anderson, H. L., Yap, J. T., Miller, M.P., Robbins, A., Jones, T., & Price, P.M. (2003). Assessment of pharmacodynamic vascular response in a phase I trial of combretastatin A4 phosphate. *Journal of clinical oncology : official journal of the American Society of Clinical Oncology* 21(15): 2823-2830, 0732-183X

Backer, M. V., Levashova, Z., Levenson, R., Blankenberg, F.G., & Backer, J. M. (2008). Cysteine-containing fusion tag for site-specific conjugation of therapeutic and imaging agents to targeting proteins. *Methods in molecular biology* 494: 275-294, 1064-3745

Backer, M. V., Patel, V., Jehning, B. T., Claffey, K. P., & Backer, J. M. (2006). Surface immobilization of active vascular endothelial growth factor via a cysteine-containing tag. *Biomaterials* 27(31): 5452-5458, 0142-9612

Barnard, S., Leen, E., Cooke, T., & Angerson, W. (2008). A contrast-enhanced ultrasound study of benign and malignant breast tissue. *South African medical journal* 98(5): 386-391, 0256-9574

Beaney, R. P., Lammertsma, A. A., Jones, T., McKenzie, C. G., & Halnan, K. E. (1984). Positron emission tomography for in-vivo measurement of regional blood flow, oxygen utilisation, and blood volume in patients with breast carcinoma. *Lancet* 1(8369): 131-134, 0140-6736

Beer, A. J., Lorenzen, S., Metz, S., Herrmann, K., Watzlowik, P., Wester, H. J., Peschel, C., Lordick, F., & Schwalger, M. (2008). Comparison of integrin alphaVbeta3 expression and glucose metabolism in primary and metastatic lesions in cancer patients: a PET study using 18F-galacto-RGD and 18F-FDG. *Journal of nuclear medicine : official publication, Society of Nuclear Medicine* 49(1): 22-29, 0161-5505

Belliveau, J. W., Rosen, B. R., Kantor, H. L., Rzedzian, R. R., Kennedy, D. N., McKinstry, R. C., Vevea, J. M., Cohen, M. S., Pykett, I. L., & Brady, T. J. (1990). Functional cerebral imaging by susceptibility-contrast NMR. *Magnetic resonance in medicine : official journal of the Society of Magnetic Resonance in Medicine / Society of Magnetic Resonance in Medicine* 14(3): 538-546, 0740-3194

Bergers, G., & Benjamin, L. E. (2003). Tumorigenesis and the angiogenic switch. *Nature reviews. Cancer* 3(6): 401-410, 1474-175X

Bernabeu, C., Lopez-Novoa, J. M., & Quintanilla, M. (2009). The emerging role of TGF-beta superfamily coreceptors in cancer. *Biochimica et biophysica acta* 1792(10): 954-973, 0006-3002

Blankenberg, F. G., Backer, M. V., Levashova, Z., Patel, V., & Backer, J. M. (2006). In vivo tumor angiogenesis imaging with site-specific labeled (99m)Tc-HYNIC-VEGF. *European journal of nuclear medicine and molecular imaging* 33(7): 841-848, 1619-7070

Blomley, M. J., Albrecht, T., Cosgrove, D. O., & Bamber, J. C. (1997). Can relative contrast agent concentration be measured in vivo with color Doppler US? *Radiology* 204(1): 279-281, 0033-8419

Bredow, S., Lewin, M., Hofmann, B., Marecos, E., & Weissleder, R. (2000). Imaging of tumour neovasculature by targeting the TGF-beta binding receptor endoglin. *European journal of cancer* 36(5): 675-681, 0959-8049

Bremer, C., Bredow, S., Mahmood, U., Weissleder, R. & Tung, C. H. (2001). Optical imaging of matrix metalloproteinase-2 activity in tumors: feasibility study in a mouse model. *Radiology* 221(2): 523-529, 0033-8419

Bremer, C., Mustafa, M., Bogdanov, A., Jr., Ntziachristos, V., Petrovsky, A., & Weissleder, R. (2003). Steady-state blood volume measurements in experimental tumors with different angiogenic burdens a study in mice. *Radiology* 226(1): 214-220, 0033-8419

Brix, G., Semmler, W., Port, R., Schad, L. R., Layer, G. & Lorenz, W. J. (1991). Pharmacokinetic parameters in CNS Gd-DTPA enhanced MR imaging. *Journal of computer assisted tomography* 15(4): 621-628, 0363-8715

Bronikowski, T. A., Dawson, C. A., & Linehan, J. H. (1983). Model-free deconvolution techniques for estimating vascular transport functions. *International journal of bio-medical computing* 14(5): 411-429, 0020-7101

Brooks, P. C., Clark, R. A., & Cheresh, D. A. (1994). Requirement of vascular integrin alpha v beta 3 for angiogenesis. *Science* 264(5158): 569-571, 0036-8075

Brown, J. M. ,& Giaccia, A. J. (1998). The unique physiology of solid tumors: opportunities (and problems) for cancer therapy. *Cancer research* 58(7): 1408-1416, 0008-5472

Cai, W., Chen, K., Li, Z. B., Gambhir, S. S., & Chen, X. (2007). Dual-function probe for PET and near-infrared fluorescence imaging of tumor vasculature. *Journal of nuclear medicine : official publication, Society of Nuclear Medicine* 48(11): 1862-1870, 0161-5505

Cai, W., Chen, K., Mohamedall, K. A., Cao, Q., Gambhir, S. S., Rosenblum, M. G., & Chen X. (2006). PET of vascular endothelial growth factor receptor expression. *Journal of nuclear medicine : official publication, Society of Nuclear Medicine* 47(12): 2048-2056, 0161-5505

Cai, W., Niu, G., & Chen, X. (2008). Imaging of integrins as biomarkers for tumor angiogenesis. *Current pharmaceutical design* 14(28): 2943-2973, 1873-4286

Cai, W., D. Shin, D. W., Chen, K., Gheysens, O., Cao, Q., Wang, S. X., Gambhir, S. S., & Chen, X. (2006). Peptide-labeled near-infrared quantum dots for imaging tumor vasculature in living subjects. *Nano letters* 6(4): 669-676, 1530-6984

Cai, W., Wu, Y., Chen, K., Cao, Q., Tice, D. A., & Chen, X. (2006). In vitro and in vivo characterization of 64Cu-labeled Abegrin, a humanized monoclonal antibody against integrin alpha v beta 3. *Cancer research* 66(19): 9673-9681, 1538-7445

Cenic, A., Nabavi, D. G., Craen, R. A., Gelb, A. W., & Lee, T. Y. (2000). A CT method to measure hemodynamics in brain tumors: validation and application of cerebral blood flow maps. *AJNR. American journal of neuroradiology* 21(3): 462-470, 0195-6108

Chen, X., Conti, P. S., & Moats, R. A. (2004). In vivo near-infrared fluorescence imaging of integrin alphavbeta3 in brain tumor xenografts. *Cancer research* 64(21): 8009-8014, 0008-5472

Cheng, Z., Wu, Y., Xiong, Z., Gambhir, S. S., & Chen, X. (2005). Near-infrared fluorescent RGD peptides for optical imaging of integrin alphavbeta3 expression in living mice. *Bioconjugate chemistry* 16(6): 1433-1441, 1043-1802

Choyke, P. L., Dwyer, A. J., & Knopp, M. V. (2003). Functional tumor imaging with dynamic contrast-enhanced magnetic resonance imaging. *Journal of magnetic resonance imaging : JMRI* 17(5): 509-520, 1053-1807

Claassen, L., Seidel, G., & Algermissen, C. (2001). Quantification of flow rates using harmonic grey-scale imaging and an ultrasound contrast agent: an in vitro and in vivo study. *Ultrasound in medicine & biology* 27(1): 83-88, 0301-5629

Cornelissen, B., Oltenfreiter, R., Kersemans, V., Staelens, L., Frankenne, F., Foidart, J. M., & Slegers, G. (2005). In vitro and in vivo evaluation of [123I]-VEGF165 as a potential tumor marker. *Nuclear medicine and biology* 32(5): 431-436, 0969-8051

Corot, C., Robert, P., Idee, J. M., & Port, M. (2006). Recent advances in iron oxide nanocrystal technology for medical imaging. *Advanced drug delivery reviews* 58(14): 1471-1504, 0169-409X

Cosgrove, D., & Lassau, N. (2010). Imaging of perfusion using ultrasound. *European journal of nuclear medicine and molecular imaging* 37 Suppl 1: S65-85, 1619-7089

Costello, B., Li, C., Duff, S., Butterworth, D., Khan, A., Perkins, M., Owens, S., Al-Mowallad, A. F., O'Dwyer, S., & Kumar, S. (2004). Perfusion of 99Tcm-labeled CD105 Mab into kidneys from patients with renal carcinoma suggests that CD105 is a promising vascular target. *International journal of cancer. Journal international du cancer* 109(3): 436-441, 0020-7136

Dennie, J., Mandeville, J. B., Boxerman, J. L., Packard, S. D., Rosen, B. R., & Weisskoff, R. M. (1998). NMR imaging of changes in vascular morphology due to tumor angiogenesis. *Magnetic resonance in medicine : official journal of the Society of Magnetic Resonance in Medicine / Society of Magnetic Resonance in Medicine* 40(6): 793-799, 0740-3194

Deshpande, N., Needles, A., & Willmann, J. K. (2010). Molecular ultrasound imaging: current status and future directions. *Clinical radiology* 65(7): 567-581, 1365-229X

Deshpande, N., Pysz, M. A., & Willmann, J. K. (2010). Molecular ultrasound assessment of tumor angiogenesis. *Angiogenesis* 13(2): 175-188, 1573-7209

Di Marco, M., Di Cicilia, R., Macchini, M., Nobili, E., Vecchiarelli, S., Brandi, G., & Biasco, G. (2010). Metastatic pancreatic cancer: is gemcitabine still the best standard treatment? (Review). *Oncology reports* 23(5): 1183-1192, 1791-2431

Eckersley, R. J., Sedelaar, J. P., Blomley, M. J., Wijkstra, H., deSouza, N. M., Cosgrove, D. O., & de la Rosette, J. J. (2002). Quantitative microbubble enhanced transrectal ultrasound as a tool for monitoring hormonal treatment of prostate carcinoma. *The Prostate* 51(4): 256-267, 0270-4137

Ellegala, D. B., Leong-Poi, H., Carpenter, J. E., Klibanov, A. L., Kaul, S., Shaffrey, M. E., Sklenar, J., & Lindner, J. R. (2003). Imaging tumor angiogenesis with contrast ultrasound and microbubbles targeted to alpha(v)beta3. *Circulation* 108(3): 336-341, 1524-4539

Enochs, W. S., Harsh, G., Hochberg, F, & Weissleder, R. (1999). Improved delineation of human brain tumors on MR images using a long-circulating, superparamagnetic iron oxide agent. *Journal of magnetic resonance imaging : JMRI* 9(2): 228-232, 1053-1807

Ferrara, N. 2004). Vascular endothelial growth factor: basic science and clinical progress. *Endocrine reviews* 25(4): 581-611, 0163-769X

Ferrara, N., & Kerbel R. S. (2005). Angiogenesis as a therapeutic target. *Nature* 438(7070): 967-974, 1476-4687

Folkman, J. (1971). Tumor angiogenesis: therapeutic implications. *The New England journal of medicine* 285(21): 1182-1186.

Folkman, J. (1995). Angiogenesis in cancer, vascular, rheumatoid and other disease. *Nature medicine* 1(1): 27-31, 1078-8956

Fonsatti, E., Altomonte, M., Arsian, P. & Maio, M. (2003). Endoglin (CD105): a target for anti-angiogenetic cancer therapy. *Current drug targets* 4(4): 291-296, 1389-4501

Fonsatti, E., Jekunen, A. P., Kairemo, K. J., Coral, S., Snellman, M., Nicotra, M. R., Natali, P. G., Altomonte, M., & Maio, M. (2000). Endoglin is a suitable target for efficient imaging of solid tumors: in vivo evidence in a canine mammary carcinoma model. *Clinical cancer research : an official journal of the American Association for Cancer Research* 6(5): 2037-2043, 1078-0432

Fournier, L. S., Oudard, S., Thiam, R., Trinquart, L., Banu, E., Medioni, J., Balvay, D., Chatellier, G., Frija, G., & Cuenod, C. A. (2010). Metastatic renal carcinoma: evaluation of antiangiogenic therapy with dynamic contrast-enhanced CT. *Radiology* 256(2): 511-518, 1527-1315

Fraioli, F., Anzidei, M., Zaccagna, F., Mennini, M. L., Serra, G., Gori, B., Longo, F., Catalano, C., & Passariello, R. (2011). Whole-tumor perfusion CT in patients with advanced lung adenocarcinoma treated with conventional and antiangiogenetic chemotherapy: initial experience. *Radiology* 259(2): 574-582, 1527-1315

Frauscher, F., Klauser, A., Berger, A. P., Halern, E. J., Feuchtner, G., Koppelstaetter, F., Pallwein, L., Pinggera, G. M., Weirich, H., Horninger, W., Bartsch, G., & zur Nedden, D. (2003). The value of ultrasound (US) in the diagnosis of prostate cancer. *Der Radiologe* 43(6): 455-463, 0033-832X

Furman-Haran, E., Margalit, R., Grobgeld, D., & Degani, H. (1996). Dynamic contrast-enhanced magnetic resonance imaging reveals stress-induced angiogenesis in MCF7 human breast tumors. *Proceedings of the National Academy of Sciences of the United States of America* 93(13): 6247-6251, 0027-8424

Goel, S., Duda, D. G., Xu, L., Munn, L. L., Boucher, Y., Fukumura, D., & Jain, R. K. (2011). Normalization of the vasculature for treatment of cancer and other diseases. *Physiological reviews* 91(3): 1071-1121.

Goh, V., Halligan, S., Daley, F., Wellsted, D. M., Guenther, T., & Bartram, C. I. (2008). Colorectal tumor vascularity: quantitative assessment with multidetector CT--do tumor perfusion measurements reflect angiogenesis? *Radiology* 249(2): 510-517, 1527-1315

Guimaraes, A. R., Rakhlin, E., Weissleder, R., & Thayer, S. P. (2008). Magnetic resonance imaging monitors physiological changes with antihedgehog therapy in pancreatic adenocarcinoma xenograft model. *Pancreas* 37(4): 440-444, 1536-4828

Guimaraes, A. R., Ross, R., Figuereido, J. L., Watermen, P., & Weissleder, R. (2011). MRI with magnetic nanoparticles monitors downstream anti-angiogenic effects of mTOR inhibition. *Molecular imaging and biology : MIB : the official publication of the Academy of Molecular Imaging* 13(2): 314-320, 1860-2002

Haubner, R. (2006). Alphavbeta3-integrin imaging: a new approach to characterise angiogenesis? *European journal of nuclear medicine and molecular imaging* 33 Suppl 1: 54-63, 1619-7070

Haubner, R., Weber, W. A., Beer, A. J., Vabuliene, E., Reim, D., Sarbia, M., Becker, K. F., Goebel, M., Hein, R., Wester, H. J., Kessler, H., & Schwaiger, M. (2005). Noninvasive visualization of the activated alphavbeta3 integrin in cancer patients by positron emission tomography and [18F]Galacto-RGD. *PLoS medicine* 2(3): e70, 1549-1676

Haubner, R., Wester, H. J., Reuning, U., Senekowitsch-Schmidtke, R., Diefenbach, B., Kessler, H., Stocklin, G., & Schwaiger, M. (1999). Radiolabeled alpha(v)beta3 integrin antagonists: a new class of tracers for tumor targeting. *Journal of nuclear medicine : official publication, Society of Nuclear Medicine* 40(6): 1061-1071, 0161-5505

Haubner, R., Wester, H. J., Weber, W. A., Mang, C., Ziegler, S. I., Goodman, S. L., Senekowitsch-Schmidtke, R., Kessler, H., & Schwaiger, M. (2001). Noninvasive imaging of alpha(v)beta3 integrin expression using 18F-labeled RGD-containing glycopeptide and positron emission tomography. *Cancer research* 61(5): 1781-1785, 0008-5472

Helmlinger, G., Yuan, F., Dellian, M., & Jain, R. K. (1997). Interstitial pH and pO2 gradients in solid tumors in vivo: high-resolution measurements reveal a lack of correlation. *Nature medicine* 3(2): 177-182, 1078-8956

Herbst, R. S., Mullani, N. A., Davis, D. W., Hess, K. R., McConkey, D. J., Charnsangavej, C., O'Reilly, M. S., Kim, H. W., Baker, C., Roach, J., Ellis, L. M., Rashid, A., Pluda, J., Bucana, C., Madden, T. L., Tran, H. T., & Abbruzzese, J. L. (2002). Development of biologic markers of response and assessment of antiangiogenic activity in a clinical trial of human recombinant endostatin. *Journal of clinical oncology : official journal of the American Society of Clinical Oncology* 20(18): 3804-3814, 0732-183X

Hulka, C. A., Edmister, W. B., Smith, B. L., Tan, L., Sgroi, D. C., Campbell, T., Kopans, D. B., & Weisskoff, R. M. (1997). Dynamic echo-planar imaging of the breast: experience in diagnosing breast carcinoma and correlation with tumor angiogenesis. *Radiology* 205(3): 837-842, 0033-8419

Hulka, C. A., Smith, B. L., Sgroi, D. C., Tan, L., Edmister, W. B., Semple, J. P., Campbell, T., Kopans, D. B., Brady, T. J., & Weisskoff, R. M. (1995). Benign and malignant breast lesions: differentiation with echo-planar MR imaging. *Radiology* 197(1): 33-38, 0033-8419

Hyodo, F., Chandramouli, G. V., Matsumoto, S., Matsumoto, K., Mitchell, J. B., Krishna, M. C., & Munasinghe, J. P. (2009). Estimation of tumor microvessel density by MRI using a blood pool contrast agent. *International journal of oncology* 35(4): 797-804, 1791-2423.

Ito, M., Lammertsma, A. A., Wise, R. J., Bernardi, S., Frackowiak, R. S., Heather, J. D., McKenzie, C. G., Thomas, D. G., & Jones, T. (1982). Measurement of regional cerebral blood flow and oxygen utilisation in patients with cerebral tumours using

15O and positron emission tomography: analytical techniques and preliminary results. *Neuroradiology* 23(2): 63-74, 0028-3940.

Izumi, Y., Xu, L., di Tomaso, E., Fukumura, D., & Jain, R. K. (2002). Tumour biology: herceptin acts as an anti-angiogenic cocktail. *Nature* 416(6878): 279-280.

Jain, R. K. (1989). Delivery of novel therapeutic agents in tumors: physiological barriers and strategies. *Journal of the National Cancer Institute* 81(8): 570-576, 0027-8874

Jain, R. K. (2001). Normalizing tumor vasculature with anti-angiogenic therapy: a new paradigm for combination therapy. *Nature medicine* 7(9): 987-989, 1078-8956

Jain, R. K. (2005). Normalization of tumor vasculature: an emerging concept in antiangiogenic therapy. *Science* 307(5706): 58-62.

Jain, R. K., Duda, D. G., Clark, J. W., & Loeffler, J. S. (2006). Lessons from phase III clinical trials on anti-VEGF therapy for cancer. *Nature clinical practice. Oncology* 3(1): 24-40, 1743-4254

Janssen, M. L., Oyen, W. J., Dijkgraaf, I., Massuger, L. F., Frielink, C., Edwards, D. S., Rajopadhye, M., Boonstra, H., Corstens, F. H., & Boerman, O. C. (2002). Tumor targeting with radiolabeled alpha(v)beta(3) integrin binding peptides in a nude mouse model. *Cancer research* 62(21): 6146-6151, 0008-5472

Jayson, G. C., Zweit, J, Jackson, A., Mulatero, C., Julyan, P., Ranson, M., Broughton, L., Wagstaff, J., Hakannson, L., Groenewegen, G., Bailey, J., Smith, N., Hastings, D., Lawrance, J., Haroon, H., Ward, T., McGown, A. T., Tang, M., Levitt, D., Marreaud, S., Lehmann, F. F., Herold, M. & Zwierzine, H. (2002). Molecular imaging and biological evaluation of HuMV833 anti-VEGF antibody: implications for trial design of antiangiogenic antibodies. *Journal of the National Cancer Institute* 94(19): 1484-1493, 0027-8874

Jiang, T., Kambadakone, A., Kulkarni, N. M., Zhu, A. X., & Sahani, D. V. (2011). Monitoring Response to Antiangiogenic Treatment and Predicting Outcomes in Advanced Hepatocellular Carcinoma Using Image Biomarkers, CT Perfusion, Tumor Density, and Tumor Size (RECIST). *Investigative radiology*, 1536-0210

Jin, Z. H., Josserand, V., Foillard, S., Boturyn, D., Dumy, P., Favrot, M. C., & Coll, J. L. (2007). In vivo optical imaging of integrin alphaV-beta3 in mice using multivalent or monovalent cRGD targeting vectors. *Molecular cancer* 6: 41, 1476-4598

Josephs, D., Spicer, J., & O'Doherty, M. (2009). Molecular imaging in clinical trials. *Targeted oncology* 4(3): 151-168, 1778-260X.

Jung, E. M., Jungius, K. P., Rupp, N., Gallegos, M., Ritter, G., Lenhart, M., Clevert, D. A., & Kubale, R. (2005). Contrast enhanced harmonic ultrasound for differentiating breast tumors - first results. *Clinical hemorheology and microcirculation* 33(2): 109-120, 1386-0291

Kedar, R. P., Cosgrove, D. o., Bamber, J. C., & Bell, D. S. (1995). Automated quantification of color Doppler signals: a preliminary study in breast tumors. *Radiology* 197(1): 39-43, 0033-8419

Klibanov, A. L. (2005). Ligand-carrying gas-filled microbubbles: ultrasound contrast agents for targeted molecular imaging. *Bioconjugate chemistry* 16(1): 9-17, 1043-1802

Klibanov, A. L. (2009). Preparation of targeted microbubbles: ultrasound contrast agents for molecular imaging. *Medical & biological engineering & computing* 47(8): 875-882, 1741-0444

Klibanov, A. L., Hughes, M. S., Villanueva, F. S., Jankowski, R. J., Wagner, W. R., Wojdyla, J. K., Wible, J. H., & Brandenburger, G. H. (1999). Targeting and ultrasound imaging of microbubble-based contrast agents. *Magma* 8(3): 177-184, 0968-5243

Knopp, M. V., Giesel, F.L., Marcos, H., von Tengg-Kobligk, H., & Choyke, P. (2001). Dynamic contrast-enhanced magnetic resonance imaging in oncology. *Topics in magnetic resonance imaging : TMRI* 12(4): 301-308, 0899-3459

Knopp, M. V., Weiss, E., Sinn, H. P., Mattern, J,. Junkermann, H., Radeleff, A., Magener, A., Brix, G., Delorme, S., Zuna, I., & van Kaick, G. (1999). Pathophysiologic basis of contrast enhancement in breast tumors. *Journal of magnetic resonance imaging : JMRI* 10(3): 260-266, 1053-1807

Kok, R. J., Schraa, A. J., Bos, E. J., Moorlag, H. E., Asgeirsdottir, S. A., Everts, M., Meijer, D. K., & Molema, G. (2002). Preparation and functional evaluation of RGD-modified proteins as alpha(v)beta(3) integrin directed therapeutics. *Bioconjugate chemistry* 13(1): 128-135, 1043-1802

Korpanty, G., Carbon, J. G., Grayburn, P. A., Fleming, J. B., & Brekken, R. A. (2007). Monitoring response to anticancer therapy by targeting microbubbles to tumor vasculature. *Clinical cancer research : an official journal of the American Association for Cancer Research* 13(1): 323-330, 1078-0432

Korpanty, G., Grayburn, P. A., Shohet, R. V., & Brekken, R. A. (2005). Targeting vascular endothelium with avidin microbubbles. *Ultrasound in medicine & biology* 31(9): 1279-1283, 0301-5629

Kossodo, S., Pickarski, M., Lin, S. A., Gleason, A., Gaspar, R., Buono, C., Ho, G., Blusztajn, A., Cuneo, G., Zhang, J., Jensen, J., Hargreaves, R., Coleman, P., Hartman, G., Rajopadhye, M., Duong le, T., Sur, C., Yared, W., Peterson, J., & Bednar, B. (2010). Dual in vivo quantification of integrin-targeted and protease-activated agents in cancer using fluorescence molecular tomography (FMT). *Molecular imaging and biology : MIB : the official publication of the Academy of Molecular Imaging* 12(5): 488-499, 1860-2002

Lee, T. Y., Purdie, T. G., & Stewart, E. (2003). CT imaging of angiogenesis. *The quarterly journal of nuclear medicine : official publication of the Italian Association of Nuclear Medicine* 47(3): 171-187, 1125-0135

Levashova, Z., Backer, M., Backer, J. M., & Blankenberg, F. G. (2008). Direct site-specific labeling of the Cys-tag moiety in scVEGF with technetium 99m. *Bioconjugate chemistry* 19(5): 1049-1054, 1520-4812

Li, S., Peck-Radosavljevic, M., Kienast, O., Preitfellner, J., Havlik, E., Schima, W., Traub-Weidinger, T., Graf, S., Beheshti, M., Schmid, M., Angelberger, P., & Dudczak, R. (2004). Iodine-123-vascular endothelial growth factor-165 (123I-VEGF165). Biodistribution, safety and radiation dosimetry in patients with pancreatic carcinoma. *The quarterly journal of nuclear medicine and molecular imaging : official publication of the Italian Association of Nuclear Medicine* 48(3): 198-206, 1824-4785

Lucidarme, O., Kono, Y., Corbell, J., Choi, S. H., & Mattrey, R. F. (2003). Validation of ultrasound contrast destruction imaging for flow quantification. *Ultrasound in medicine & biology* 29(12): 1697-1704, 0301-5629

Ma, X., Labinaz, M., Goldstein, J., Miller, H., Keon, W. J., Letarte, M., & O'Brien, E. (2000). Endoglin is overexpressed after arterial injury and is required for transforming

growth factor-beta-induced inhibition of smooth muscle cell migration. *Arteriosclerosis, thrombosis, and vascular biology* 20(12): 2546-2552, 1524-4636

Mankoff, D. A. (2007). A definition of molecular imaging. *Journal of nuclear medicine : official publication, Society of Nuclear Medicine* 48(6): 18N, 21N, 0161-5505

Massoud, T. F., & Gambhir S. S. (2003). Molecular imaging in living subjects: seeing fundamental biological processes in a new light. *Genes & development* 17(5): 545-580, 0890-9369

Miles, K. A., & Griffiths, M. R. (2003). Perfusion CT: a worthwhile enhancement? *The British journal of radiology* 76(904): 220-231, 0007-1285

Millauer, B., Wizigmann-Voos, S., Schnurch, H., Martinez, R., Moller, N. P., Risau, W., & Ullrich, A. (1993). High affinity VEGF binding and developmental expression suggest Flk-1 as a major regulator of vasculogenesis and angiogenesis. *Cell* 72(6): 835-846, 0092-8674

Monzani, E., & and La Porta, C. A. (2008). Targeting cancer stem cells to modulate alternative vascularization mechanisms. *Stem cell reviews* 4(1): 51-56.

Morgan, B., Thomas, A. L., Drevs, J., Hennig, J., Buchert, M., Jivan, A., Horsfield, M. A., Mross, K., Ball, H. A., Lee, L., Mietlowski, W., Fuxuis, S., Unger, C., O'Byrne, K., Henry, A., Cherryman, G. R., Laurent, D., Dugan, M., Marme, D., & Steward, W. P. (2003). Dynamic contrast-enhanced magnetic resonance imaging as a biomarker for the pharmacological response of PTK787/ZK 222584, an inhibitor of the vascular endothelial growth factor receptor tyrosine kinases, in patients with advanced colorectal cancer and liver metastases: results from two phase I studies. *Journal of clinical oncology : official journal of the American Society of Clinical Oncology* 21(21): 3955-3964, 0732-183X

Mulder, W. J., Castermans, K., van Beijnum, J. R., Oude Egbrink, M. G., Chin, P. T., Fayad, Z. A., Lowik, C. W., Kaijzel, E. L., Que, I., Storm, G., Strijkers, G. J., Griffioen, A. W., & Nicolay, K. (2009). Molecular imaging of tumor angiogenesis using alphavbeta3-integrin targeted multimodal quantum dots. *Angiogenesis* 12(1): 17-24, 1573-7209

Mulder, W. J., Koole, R., Brandwijk, R. J., Storm, G., Chin, P. T., Strijkers, G. J., de Mello Donega, C., Nicolay, K., & Griffioen, A. W. (2006). Quantum dots with a paramagnetic coating as a bimodal molecular imaging probe. *Nano letters* 6(1): 1-6, 1530-6984

Mulder, W. J., Strijkers, G. J., Habets, J. W., Bleeker, E. J., van der Schaft, D. W., Storm, G., Koning, G. A., Griffioen, A. W., & Nicolay, K. (2005). MR molecular imaging and fluorescence microscopy for identification of activated tumor endothelium using a bimodal lipidic nanoparticle. *The FASEB journal : official publication of the Federation of American Societies for Experimental Biology* 19(14): 2008-2010, 1530-6860

Ostergaard, L., Smith, D. F., Vestergaard- Poulsen, P., Hansen, S. B., Gee, A. D., Gjedde, A., & Gyldensted, C. (1998). Absolute cerebral blood flow and blood volume measured by magnetic resonance imaging bolus tracking: comparison with positron emission tomography values. *Journal of cerebral blood flow and metabolism : official journal of the International Society of Cerebral Blood Flow and Metabolism* 18(4): 425-432, 0271-678X

Padera, T. P., Stoll, B. R., Tooredman, J. B., Capen, D., di Tomaso, E., & Jain, R. K. (2004). Pathology: cancer cells compress intratumour vessels. *Nature* 427(6976): 695, 1476-4687

Pathak, A. P., M. Penet, et al. (2010). MR Molecular Imaging of Tumor Vasculature and Vascular Targets. *Advances in Genetics*, Elsevier Inc. 69.

Patlak, C. S., Blasberg, R. G., & Fenstermacher, J. D. (1983). Graphical evaluation of blood-to-brain transfer constants from multiple-time uptake data. *Journal of cerebral blood flow and metabolism : official journal of the International Society of Cerebral Blood Flow and Metabolism* 3(1): 1-7, 0271-678X

Perkins, A. C., Frier, M., Hindle, A. J., Blackshaw, P. E., Bailey, S. E., Hebden, J. M., Middleton, S. M., & Wastie, M. L. (1997). Human biodistribution of an ultrasound contrast agent (Quantison) by radiolabelling and gamma scintigraphy. The *British journal of radiology* 70(834): 603-611, 0007-1285

Persigehl, T., Bieker, R., Matuszewski, L., Wall, A., Kessler, T., Kooijman, H., Meier, N., Ebert, W., Berdel, W. E., Heindel, W., Mesters, R. M., & Bremer, C. (2007). Antiangiogenic tumor treatment: early noninvasive monitoring with USPIO-enhanced MR imaging in mice. *Radiology* 244(2): 449-456, 0033-8419

Petralia, G., Preda, L., D'Andrea, G., Viotti, S., Bonello, L., De Filippi, R., & Bellomi, M. (2010). CT perfusion in solid-body tumours. Part I: Technical issues. *La Radiologia medica* 115(6): 843-857, 1826-6983

Pham, C. D., Roberts, T. P., van Bruggen, N., Melnyk, O., Mann, J., Ferrara, N., Cohen, R. L., & Brasch, R. C. (1998). Magnetic resonance imaging detects suppression of tumor vascular permeability after administration of antibody to vascular endothelial growth factor. *Cancer investigation* 16(4): 225-230, 0735-7907

Piccoli, C. W. (1997). Contrast-enhanced breast MRI: factors affecting sensitivity and specificity. *European radiology* 7 Suppl 5: 281-288, 0938-7994

Pochon, S., Tardy, I., Bussat, P., Bettinger, T., Brochot, J., von Wronski, M., Passantino, L., & Schneider, M. (2010). BR55: a lipopeptide-based VEGFR2-targeted ultrasound contrast agent for molecular imaging of angiogenesis. *Investigative radiology* 45(2): 89-95, 1536-0210

Purdie, T. G., Henderson, E., & Lee, T. Y. (2001). Functional CT imaging of angiogenesis in rabbit VX2 soft-tissue tumour. *Physics in medicine and biology* 46(12): 3161-3175, 0031-9155

Pysz, M. A., Foygel, K., Rosenberg, J., Gambhir, S. S., Schneider, M., & Willmann, J. K. (2010). Antiangiogenic cancer therapy: monitoring with molecular US and a clinically translatable contrast agent (BR55). *Radiology* 256(2): 519-527, 1527-1315

Ring, J., Persigehl, T., Remmele, S., Heindel, W., Dahnke, H., & Bremer, C. (2011). Monitoring of bevacizumab-induced antiangiogenic treatment effects by "steady state" ultrasmall superparamagnetic iron oxide particles magnetic resonance imaging using robust multiecho DeltaR2* relaxometry. *Investigative radiology* 46(5): 326-330, 1536-0210

Rizzatto, G., Martegani, A, Chersevani, R., Macorig, D., Vrtovec, M. Aiani, L., & Tufarulo, L. (2001). Importance of staging of breast cancer and role of contrast ultrasound. *European radiology* 11 Suppl 3: E47-51, 0938-7994

Sabir, A., Schor-Bardach, R., Wilcox, C. J., Rahmanuddin, S., Atkins, M. B., Kruskal, J. B., Signoretti, S., Raptopoulos, V. D., & Goldberg, S. N. (2008). Perfusion MDCT enables early detection of therapeutic response to antiangiogenic therapy. *AJR. American journal of roentgenology* 191(1): 133-139, 1546-3141

Saltz, L. B., Clarke, S., Diaz-Rubio, E., Scheithauer, W., Figer, A., Wong, R., Koski, S., Lichinitser, M., Yang, T. S., Rivera, F., Couture, F., Sirzen, F., & Cassidy, J. (2008). Bevacizumab in combination with oxaliplatin-based chemotherapy as first-line therapy in metastatic colorectal cancer: a randomized phase III study. *Journal of clinical oncology : official journal of the American Society of Clinical Oncology* 26(12): 2013-2019, 1527-7755

Sandler, A., Gray, R., Perry, M. C., Brahmer, J., Schiller, J. H., Dowlati, A., Lilenbaum, R., & Johnson, D. H. (2006). Paclitaxel-carboplatin alone or with bevacizumab for non-small-cell lung cancer. *The New England journal of medicine* 355(24): 2542-2550, 1533-4406

Schmieder, A. H., Winter, P. M., Caruthers, S. D., Harris, T. D., Williams, T. A., Allen, J. S., Lacy, E. K., Zhang, H., Scott, M. J., Hu, G., Robertson, J. D., Wickline, S. A., & Lanza, G. M. (2005). Molecular MR imaging of melanoma angiogenesis with alphanubeta3-targeted paramagnetic nanoparticles. *Magnetic resonance in medicine : official journal of the Society of Magnetic Resonance in Medicine / Society of Magnetic Resonance in Medicine* 53(3): 621-627, 0740-3194

Schraa, A. J., Kok, R. J., Moorlag, H. E., Bos, E. J., Proost, J. H., Meijer, D. K., de Leij, L. F., & Molema, G. (2002). Targeting of RGD-modified proteins to tumor vasculature: a pharmacokinetic and cellular distribution study. *International journal of cancer. Journal international du cancer* 102(5): 469-475, 0020-7136

Shiyan, L., Pintong, H., Zongmin, W., Fuguang, H., Zhiqiang, Z., Yan, Y., & Cosgrove, D. (2009). The relationship between enhanced intensity and microvessel density of gastric carcinoma using double contrast-enhanced ultrasonography. *Ultrasound in medicine & biology* 35(7): 1086-1091, 1879-291X

Sipkins, D. A., Cheresh, D. A., Kazemi, M. R., Nevin, L. M., Bednarski, M. D., & Li, K. C. (1998). Detection of tumor angiogenesis in vivo by alphaVbeta3-targeted magnetic resonance imaging. *Nature medicine* 4(5): 623-626, 1078-8956

Stohrer, M., Boucher, Y., Stangassinger, M., & Jain, R. K. (2000). Oncotic pressure in solid tumors is elevated. *Cancer research* 60(15): 4251-4255, 0008-5472

Stollman, T. H., Ruers, T. J., Oyen, W. J., & Boerman, O. C. (2009). New targeted probes for radioimaging of angiogenesis. *Methods* 48(2): 188-192, 1095-9130

Su, M. Y., Cheung, Y. C., Fruehauf, J. P., Yu, H., Nalcioglu, O., Mechetner, E., Kyshtoobayeva, A., Chen, S. C., Hsueh, S., McLaren, C. E., & Wan, Y. L. (2003). Correlation of dynamic contrast enhancement MRI parameters with microvessel density and VEGF for assessment of angiogenesis in breast cancer. *Journal of magnetic resonance imaging : JMRI* 18(4): 467-477, 1053-1807

Tabata, M., Kondo, M., Haruta, Y., & Seon, B. K. (1999). Antiangiogenic radioimmunotherapy of human solid tumors in SCID mice using (125)I-labeled anti-endoglin monoclonal antibodies. *International journal of cancer. Journal international du cancer* 82(5): 737-742, 0020-7136

Teicher, B. A. (1996). A systems approach to cancer therapy. (Antioncogenics + standard cytotoxics-->mechanism(s) of interaction). *Cancer metastasis reviews* 15(2): 247-272, 0167-7659

Tofts, P. S. (1997). Modeling tracer kinetics in dynamic Gd-DTPA MR imaging. *Journal of magnetic resonance imaging : JMRI* 7(1): 91-101, 1053-1807

Tofts, P. S., Brix, G, Buckley, D. L., Evelhoch, J. L., Henderson, E., Knopp, M. V., Larsson, H. B., Lee, T. Y., Mayr, N. A., Parker, G. J., Port, R. E., Taylor, J., & Weisskoff, R. M. (1999). Estimating kinetic parameters from dynamic contrast-enhanced T(1)-weighted MRI of a diffusable tracer: standardized quantities and symbols. *Journal of magnetic resonance imaging : JMRI* 10(3): 223-232, 1053-1807

Tong, R. T., Boucher, Y., Kozin, S. V., Winkler, F., Hicklin, D. J., & Jain, R. K. (2004). Vascular normalization by vascular endothelial growth factor receptor 2 blockade induces a pressure gradient across the vasculature and improves drug penetration in tumors. *Cancer research* 64(11): 3731-3736, 0008-5472

Tropres, I., Grimault, S., Vaeth, A., Grillon, E., Julien, C., Payen, J. F., Lamalle, L., & Decorps, M. (2001). Vessel size imaging. *Magnetic resonance in medicine : official journal of the Society of Magnetic Resonance in Medicine / Society of Magnetic Resonance in Medicine* 45(3): 397-408, 0740-3194

Vag, T., Schramm, T., Kaiser, W. A., & Hilger, I. (2009). Proliferating and quiescent human umbilical vein endothelial cells (HUVECs): a potential in vitro model to evaluate contrast agents for molecular imaging of angiogenesis. *Contrast media & molecular imaging* 4(4): 192-198, 1555-4317

van der Flier, A., & Sonnenberg, A. (2001). Function and interactions of integrins. *Cell and tissue research* 305(3): 285-298, 0302-766X

van der Schaft, D. W., Seftor, R. E., Seftor, E. A., Hess, A. R., Gruman, L. M., Kirschmann, D. A., Yokoyama, Y., Griffioen, A. W., & Hendrix, M. J. (2004). Effects of angiogenesis inhibitors on vascular network formation by human endothelial and melanoma cells. *Journal of the National Cancer Institute* 96(19): 1473-1477.

van Hagen, P. M., Breeman, W. A., Bernard, H. F., Schaar, M., Mooij, C. M., Srinivasan, A., Schmidt, M. A., Krenning, E. P., & de Jong, M. (2000). Evaluation of a radiolabelled cyclic DTPA-RGD analogue for tumour imaging and radionuclide therapy. *International journal of cancer. Journal international du cancer* 90(4): 186-198, 0020-7136

Wang, H., Cai, W., Chen, K., Li, Z. B., Kashefi, A., He, L., & Chen, X. (2007). A new PET tracer specific for vascular endothelial growth factor receptor 2. *European journal of nuclear medicine and molecular imaging* 34(12): 2001-2010, 1619-7070

Wang, J., Lv, F., Fei, X., Cui, Q., Wang, L., Gao, X., Yuan, Z., Lin, Q., Lv, Y., & Liu, A. (2011). Study on the characteristics of contrast-enhanced ultrasound and its utility in assessing the microvessel density in ovarian tumors or tumor-like lesions. *International journal of biological sciences* 7(5): 600-606, 1449-2288

Wei, K., Jayaweera, A. R., Firoozan, S., Linka, A., Skyba, D. M., & Kaul, S. (1998). Quantification of myocardial blood flow with ultrasound-induced destruction of microbubbles administered as a constant venous infusion. *Circulation* 97(5): 473-483, 0009-7322

Weskott, H. P. (2008). Emerging roles for contrast-enhanced ultrasound. *Clinical hemorheology and microcirculation* 40(1): 51-71, 1386-0291

Willett, C. G., Boucher, Y., di Tomaso, E., Duda, D. G., Munn, L. L., Tong, R. T., Chung, D. C., Sahani, D. V., Kalva, S. P., Kozin, S. V., Mino, M., Cohen, K. S., Scadden, D. T., Hartford, A. C., Fischman, A. J., Clark, J. W., Ryan, D. P., Zhu, A. X., Blaszkowsky, L. S., Chen, H. X., Shellito, P. C., Lauwers, G. Y., & Jain, R. K. (2004). Direct evidence that the VEGF-specific antibody bevacizumab has antivascular effects in human rectal cancer. *Nature medicine* 10(2): 145-147, 1078-8956

Willmann, J. K., Cheng, Z., Davis, C., Lutz, A. M., Schipper, M. L., Nielsen, C. H., & Gambhir, S. S. (2008). Targeted microbubbles for imaging tumor angiogenesis: assessment of whole-body biodistribution with dynamic micro-PET in mice. *Radiology* 249(1): 212-219, 1527-1315

Willmann, J. K., Paulmurugan, R., Chen, K., Gheysens, O., Rodriguez-Porcel, M., Lutz, A. M., Chen, I. Y., Chen, X., & Gambhir, S. S. (2008). US imaging of tumor angiogenesis with microbubbles targeted to vascular endothelial growth factor receptor type 2 in mice. *Radiology* 246(2): 508-518, 1527-1315

Wink, M., Frauscher, F., Cosgrove, D., Chapelon, J. Y., Palwein, L., Mitterberger, M., Harvey, C., Rouviere, O., de la Rosette, J., & Wijkstra, H. (2008). Contrast-enhanced ultrasound and prostate cancer; a multicentre European research coordination project. *European urology* 54(5): 982-992, 0302,2838

Winter, P. M., Caruthers, S. D., Kassner, A., Harris, T. D., Chinen, L. K., Allen, J. S., lacy, E. K., Zhang, H., Robertson, J. D., Wickline, S. A., & Lanza, G. M. (2003). Molecular imaging of angiogenesis in nascent Vx-2 rabbit tumors using a novel alpha(nu)beta3-targeted nanoparticle and 1.5 tesla magnetic resonance imaging. *Cancer research* 63(18): 5838-5843, 0008-5472

Wouters, B. G., & Brown, J. M. (1997). Cells at intermediate oxygen levels can be more important than the "hypoxic fraction" in determining tumor response to fractionated radiotherapy. *Radiation research* 147(5): 541-550, 0033-7587

Wu, Y., Cai, W., & Chen, X. (2006). Near-infrared fluorescence imaging of tumor integrin alpha v beta 3 expression with Cy7-labeled RGD multimers. *Molecular imaging and biology : MIB : the official publication of the Academy of Molecular Imaging* 8(4): 226-236, 1536-1632

Yoon, S. S., Duda, D. G., Karl, D. L., Kim, T. M., Kambadakone, A. R., Chen, Y. L., Rothrock, C., Rosenberg, A. E., Nielsen, G. P., Kirsch, D. G., Choy, E., Harmon, D. C., Hornicek, F. J., Dreyfuss, J., Ancukiewicz, M., Sahani, D. V., Park, P. J., Jain, R. K., & Delaney, T. F. (2010). Phase II Study of Neoadjuvant Bevacizumab and Radiotherapy for Resectable Soft Tissue Sarcomas. *International journal of radiation oncology, biology, physics,* 1879-355X

Zhang, C., Jugold, M., Woenne, E. C., Lammers, T., Morgenstern, B., Mueller, M. M., Zentgraf, H., Bock, M., Eisenhut, M., Semmler, W., & Kiessling, F. (2007). Specific targeting of tumor angiogenesis by RGD-conjugated ultrasmall superparamagnetic iron oxide particles using a clinical 1.5-T magnetic resonance scanner. *Cancer research* 67(4): 1555-1562, 0008-5472

Zhang, D., Feng, X. Y., Henning, T. D., Wen, L., Lu, W. Y., Pan, H., Wu, X., & Zou, L. G. (2009). MR imaging of tumor angiogenesis using sterically stabilized Gd-DTPA liposomes targeted to CD105. *European journal of radiology* 70(1): 180-189.

Zhang, X., Xiong, Z., Wu, Y., Cai, W., Tseng, J. R., Gambhir, S. S., & Chen, X. (2006). Quantitative PET imaging of tumor integrin alphavbeta3 expression with 18F-FRGD2. *Journal of nuclear medicine : official publication, Society of Nuclear Medicine* 47(1): 113-121, 0161-5505

Zhu, A. X., Sahani, D. V., Duda, D. G., di Tomaso, E., Ancukiewicz, M., Catalano, O. A., Sindhwani, V., Blaszkowsky, L. S., Yoon, S. S., Lahdenranta, J., Bhargava, P., Meyerhardt, J., Clark, J. W., Kwak, E. L., Hezel, A. F., Miksad, R., Abrams, T. A., Enzinger, P. C., Fuchs, C. S., Ryan, D. P., & Jain, R. K. (2009). Efficacy, safety, and

potential biomarkers of sunitinib monotherapy in advanced hepatocellular carcinoma: a phase II study. *Journal of clinical oncology : official journal of the American Society of Clinical Oncology* 27(18): 3027-3035, 1527-7755

Zhuang, H., Yang, Z. G., Chen, H. J., Peng, Y. L., & Li, L. (2011). Time-intensity curve parameters in colorectal tumours measured using double contrast-enhanced ultrasound: correlations with tumour angiogenesis. *Colorectal disease : the official journal of the Association of Coloproctology of Great Britain and Ireland*, 1463-1318

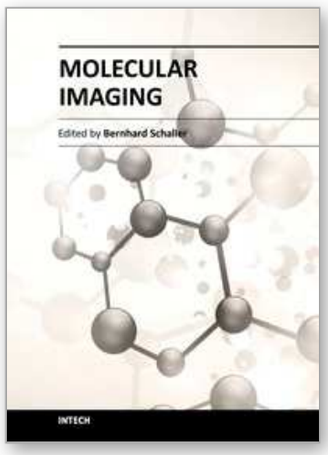

Molecular Imaging

Edited by Prof. Bernhard Schaller

ISBN 978-953-51-0359-2
Hard cover, 390 pages
Publisher InTech
Published online 16, March, 2012
Published in print edition March, 2012

The present book gives an exceptional overview of molecular imaging. Practical approach represents the red thread through the whole book, covering at the same time detailed background information that goes very deep into molecular as well as cellular level. Ideas how molecular imaging will develop in the near future present a special delicacy. This should be of special interest as the contributors are members of leading research groups from all over the world.

InTech Europe
University Campus STeP Ri
Slavka Krautzeka 83/A
51000 Rijeka, Croatia
Phone: +385 (51) 770 447
Fax: +385 (51) 686 166
www.intechopen.com

InTech China
Unit 405, Office Block, Hotel Equatorial Shanghai
No.65, Yan An Road (West), Shanghai, 200040, China
中国上海市延安西路65号上海国际贵都大饭店办公楼405单元
Phone: +86-21-62489820
Fax: +86-21-62489821

IntechOpen